

Electron and Muon production cross sections in quasielastic $\nu(\bar{\nu})$ -Nucleus scattering for $E_\nu < 1$ GeV

F. Akbar, M. Rafi Alam, M. Sajjad Athar, S. Chauhan, S. K. Singh and F. Zaidi*

Department of Physics, Aligarh Muslim University, Aligarh-202 002, India

(Dated: March 20, 2019)

In this work, we have studied (anti)neutrino induced charged current quasielastic scattering from some nuclear targets in the energy region of $E_\nu < 1$ GeV. Our aim is to confront electron and muon production cross sections relevant for $\nu_\mu \leftrightarrow \nu_e$ or $\bar{\nu}_\mu \leftrightarrow \bar{\nu}_e$ oscillation experiments. The effects due to lepton mass and its kinematic implications, radiative corrections, second class currents and uncertainties in the axial and pseudoscalar form factors are calculated for (anti)neutrino induced reaction cross sections on free nucleon as well as the nucleons bound in a nucleus where nuclear medium effects influence the cross section. For the nuclear medium effects we have taken some versions of Fermi gas model(FGM) available in literature. The results for (anti)neutrino-nucleus scattering cross section per interacting nucleons are compared with the corresponding results in free nucleon case.

PACS numbers: 12.15.Lk, 12.15.-y, 13.15+g, 13.60Rj, 21.60.Jz, 24.10Cn, 25.30Pt

I. INTRODUCTION

With the measurement of θ_{13} at the nuclear reactors [1–3] and finding a clear evidence for $\bar{\nu}_e$ disappearance, now the emphasis is upon determining mass hierarchy in the neutrino sector as well as to find signals of CP violation in the leptonic sector [4, 5]. For these physics goals, accelerator experiments like T2K [6], NO ν A [7], etc. are taking data and looking for $\nu_\mu \leftrightarrow \nu_e$ or $\bar{\nu}_\mu \leftrightarrow \bar{\nu}_e$ oscillation signals and experiments like LBNO [8], T2HK [9, 10], etc. are planned. Most of these oscillation experiments are being performed in the (anti)neutrino energy region of ~ 1 GeV. In this energy region the major contribution to the event rates comes from the charged current quasielastic(CCQE) lepton production process followed by charged current induced one pion production process. Besides these processes, $|\Delta S|=1$ processes also contribute but they are Cabibbo suppressed, while strangeness conserving $|\Delta S|=0$ processes are suppressed due to the threshold effect. The contribution to the lepton event rates from the deep inelastic scattering is expected to be small. The importance of CCQE lepton production process is two fold. Firstly, the observation of charged lepton in the final state is the cleanest signature of a (anti)neutrino interaction and secondly this is the simplest process using which energies of the incoming (anti)neutrinos may be determined. However, there are theoretical uncertainties involved while inferring the energy of neutrinos even from CCQE processes on nuclear targets and this has been discussed in detail recently by many authors [11–18].

In the electron and muon (anti)neutrinos processes, the contribution to the cross section from CCQE process would be different for the production of electrons and muons, due to lepton mass and other effects even in the presence of the universality of weak interaction. Recently, Day and McFarland [19] studied the effect of lepton mass, radiative corrections and uncertainties in the nucleon electroweak form factors including the second class currents(SCC) on the (anti)neutrino CCQE scattering cross sections from the nucleon targets. In their work, it has been shown that the radiative corrections at the tree level CCQE process may lead to important difference between electron and muon production cross sections [19], as it is proportional to $\log(\frac{E_l^*}{m_l})$, where E_l^* is the outgoing lepton energy in the center of mass frame and m_l is the mass of the charged lepton. Furthermore, the variation in the axial dipole mass M_A which has been recently discussed in literature will also lead to difference in electron and muon cross sections. The variation in the experimental measurements of M_A has been recently found out to be quite large i.e. 0.99 GeV to 1.35 GeV [20–29], from the world average $(1.026 \pm 0.021$ GeV) [30]. A change of 10% in the value of M_A say from 1 GeV to 1.1 GeV would result in almost an increase of 10% in the CCQE scattering cross section. Generally, the pseudoscalar form factor $F_P(Q^2)$ is expressed in terms of axial vector form factor $F_A(Q^2)$ using the Goldberger-Trieman relation and PCAC. However, other parameterizations of the pseudoscalar form factor $F_P(Q^2)$ based on Chiral Perturbation Theory and Lattice calculations have also been discussed in literature [31–35]. Moreover, if one considers the presence of second class currents, then there would be additional contribution to the (anti)neutrino nucleon cross sections due to the form factors $F_3^V(Q^2)$, $F_3^A(Q^2)$ associated with them. The inclusion or noninclusion of these contributions may translate into the systematic uncertainties in the determination of event rates. Some of these effects have not

* Corresponding author: zaidi.physics@gmail.com

been taken into account in the (anti)neutrino Monte Carlo generators like GENIE [36], NEUT [37], NUANCE [38], NuWro [39], GiBUU [40], etc.

In almost all the present generation (anti)neutrino experiments, moderate to heavy nuclear targets like ^{12}C , ^{16}O , ^{40}Ar , ^{56}Fe , ^{208}Pb , etc. are being used. Recently, the measurements have been performed for Q^2 distribution [20–25], double-differential scattering cross section [22, 24, 26] and total scattering cross sections [21, 22, 24, 26, 27] using some of these nuclear targets. In these nuclear targets nuclear medium effects play an important role and the effect has been found to be substantial in the low energy region. Most of the present generation Monte Carlo generators are using relativistic Fermi gas model given by Smith and Moniz [41] or the model discussed by Llewellyn Smith [42]. However, there are other variants of Fermi gas model available in literature like that of Gaisser and O'Connell [43], Singh and Oset [44, 45], Nieves et al. [46], etc. which have been applied to study (anti)neutrino-nucleus reactions. In addition to these works many other theoretical models like superscaling approach[47], mean field approximation [48], relativistic meson-nucleon model [49], relativistic Green's function model [50], plane wave impulse approximation(PWIA) [51, 52], distorted wave impulse approximation(DWIA) [53], etc., have been used in literature. Moreover, in the context of Fermi gas models the effect of two particle-two hole(2p-2h) correlation, meson exchange currents and multinucleon mechanism have also been considered in literature [54–57]. These studies have been recently summarized in some review articles [13, 58, 59], but they have not been incorporated into the present Monte Carlo generators being used in the neutrino oscillation experiments [60].

In the present work, we have studied ν_l , $\bar{\nu}_l$; ($l = e, \mu$) induced CCQE scattering from some nuclear targets like ^{12}C , ^{40}Ar , ^{56}Fe and ^{208}Pb in the energy region of $E_\nu < 1 \text{ GeV}$ including the effect due to lepton mass and its kinematic implications, radiative correction, form factors, second class currents, etc. We have performed the calculations using Local Fermi Gas Model(LFG) [61–64] and also compared the numerical results with the different Fermi gas models of Smith and Moniz [41], Llewellyn Smith [42], Gaisser and O'Connell [43]. Using the different nuclear models we have studied the difference in the lepton(electron vs muon) cross sections due to the axial dipole mass, pseudoscalar form factor, radiative corrections and effect of second class currents. Furthermore, in the Local Fermi Gas Model [61, 62] we have also included the nucleon-nucleon interactions due to which response of electroweak transition strength is modified. These modifications are calculated by incorporating the interactions of particle-hole(1p-1h) excitation in the nuclear medium in a random phase approximation(RPA) [44, 46]. Our aim of this work is to study the role of dominant nuclear medium effects like Fermi motion, binding energy and nucleon correlations on the various physics inputs which lead to difference in electron and muon scattering cross sections in the case of per nucleon target as discussed by Day and McFarland [19]. In view of this, the effect of 2p-2h, meson exchange currents and multinucleon mechanism have not been considered. This is at present beyond the scope of this paper and it may be studied as a separate work. In section-II, we present the formalism in brief, in section-III, results and discussions are presented and the findings are summarized in section IV.

II. FORMALISM

The basic reaction for the quasielastic process is a (anti)neutrino interacting with a (proton)neutron target given by

$$\left. \begin{aligned} \nu_l(k) + n(p) &\rightarrow l^-(k') + p(p') \\ \bar{\nu}_l(k) + p(p) &\rightarrow l^+(k') + n(p') \end{aligned} \right\} \quad l = e, \mu \quad (1)$$

where k , k' are the four momenta of incoming and outgoing lepton and p , p' are the four momenta of initial and final nucleon, respectively. The invariant matrix element for the charged current reaction of (anti)neutrino, given by Eq.(1) is written as

$$\mathcal{M} = \frac{G_F}{\sqrt{2}} \cos \theta_c \ l_\mu \ J^\mu \quad (2)$$

where G_F is the Fermi coupling constant ($=1.16639 \times 10^{-5} \text{ GeV}^{-2}$), θ_c ($= 13.1^0$) is the Cabibbo angle. The leptonic weak current is given by

$$l_\mu = \bar{u}(k') \gamma_\mu (1 \pm \gamma_5) u(k), \quad (3)$$

where (+ve)–ve sign is for (antineutrino)neutrino. J^μ is the hadronic current given by

$$J^\mu = \bar{u}(p') \Gamma^\mu u(p), \quad (4)$$

with

$$\begin{aligned}\Gamma^\mu &= F_1^V(Q^2)\gamma^\mu + F_2^V(Q^2)i\sigma^{\mu\nu}\frac{q_\nu}{2M} + F_3^V(Q^2)\frac{q^\mu}{M} \\ &+ F_A(Q^2)\gamma^\mu\gamma^5 + F_P(Q^2)\frac{q^\mu}{M}\gamma^5 + F_3^A(Q^2)\frac{(p+p')^\mu}{M}\gamma^5,\end{aligned}\quad (5)$$

$Q^2 (= -q^2) > 0$ is the four momentum transfer square and M is the nucleon mass. $F_{1,2}^V(Q^2)$ are the isovector vector form factors and $F_A(Q^2)$, $F_P(Q^2)$ are the axial and pseudoscalar form factors, respectively. $F_3^V(Q^2)$ and $F_3^A(Q^2)$ are the form factors related with second class current. Using the leptonic and hadronic currents given in Eq.(3) and Eq.(4), the matrix element square is obtained by using Eq.(2) as

$$|\mathcal{M}|^2 = \frac{G_F^2}{2} \cos^2 \theta_c \ L_{\mu\nu} J^{\mu\nu} \quad (6)$$

$L_{\mu\nu}$ is the leptonic tensor calculated to be

$$L_{\mu\nu} = \bar{\Sigma} \Sigma l_\mu^\dagger l_\nu = L_{\mu\nu}^{S(\nu)} \pm i L_{\mu\nu}^{A(\nu)}, \quad \text{where} \quad (7)$$

$$\begin{aligned}L_{\mu\nu}^S &= 8 [k_\mu k'_\nu + k'_\mu k_\nu - g_{\mu\nu} k \cdot k'] \quad \text{and} \\ L_{\mu\nu}^A &= 8 \epsilon_{\mu\nu\alpha\beta} k'^\alpha k^\beta,\end{aligned}\quad (8)$$

where the + sign(– sign) is for neutrino(antineutrino).

The hadronic tensor $J^{\mu\nu}$ is given by:

$$\begin{aligned}J^{\mu\nu} &= \bar{\Sigma} \Sigma J^{\mu\dagger} J^\nu \\ &= \frac{1}{2} \text{Tr} [(\not{p}' + M)\Gamma^\mu (\not{p} + M)\tilde{\Gamma}^\nu]\end{aligned}\quad (9)$$

where $\tilde{\Gamma}^\nu = \gamma^0 \Gamma^{\nu\dagger} \gamma^0$.

The hadronic current contains isovector vector form factors $F_{1,2}^V(Q^2)$ of the nucleons, which are given as

$$F_{1,2}^V(Q^2) = F_{1,2}^p(Q^2) - F_{1,2}^n(Q^2) \quad (10)$$

where $F_1^{p(n)}(Q^2)$ and $F_2^{p(n)}(Q^2)$ are the Dirac and Pauli form factors of proton(neutron) which in turn are expressed in terms of the experimentally determined Sach's electric $G_E^{p,n}(Q^2)$ and magnetic $G_M^{p,n}(Q^2)$ form factors as

$$F_1^{p,n}(Q^2) = \left(1 + \frac{Q^2}{4M^2}\right)^{-1} \left[G_E^{p,n}(Q^2) + \frac{Q^2}{4M^2} G_M^{p,n}(Q^2) \right] \quad (11)$$

$$F_2^{p,n}(Q^2) = \left(1 + \frac{Q^2}{4M^2}\right)^{-1} [G_M^{p,n}(Q^2) - G_E^{p,n}(Q^2)] \quad (12)$$

$G_E^{p,n}(Q^2)$ and $G_M^{p,n}(Q^2)$ are taken from BBBA05 [65] parameterization.

The isovector axial form factor is obtained from the quasielastic neutrino and antineutrino scattering as well as from pion electroproduction data and is parameterized as

$$F_A(Q^2) = F_A(0) \left[1 + \frac{Q^2}{M_A^2}\right]^{-2}; \quad F_A(0) = -1.267. \quad (13)$$

The pseudoscalar form factor is determined by using PCAC which gives a relation between $F_P(Q^2)$ and pion-nucleon form factor $g_{\pi NN}$, and is given by [42]:

$$F_P(Q^2) = \frac{2M^2 F_A(0)}{Q^2} \left(\frac{F_A(Q^2)}{F_A(0)} - \frac{m_\pi^2}{(m_\pi^2 + Q^2)} \frac{g_{\pi NN}(Q^2)}{g_{\pi NN}(0)} \right), \quad (14)$$

where m_π is the pion mass and $g_{\pi NN}(0)$ is the pion-nucleon strong coupling constant.

$F_P(Q^2)$ is dominated by the pion pole and is given in terms of axial vector form factor $F_A(Q^2)$ using the Goldberger-Treiman(GT) relation [42]

$$F_P(Q^2) = \frac{2M^2 F_A(Q^2)}{m_\pi^2 + Q^2}. \quad (15)$$

The form of pseudoscalar form factor $F_P(Q^2)$ using PCAC may also be written as [34]

$$F_p(Q^2) = \frac{M}{Q^2} \left[\left(\frac{2m_\pi^2 F_\pi}{m_\pi^2 + Q^2} \right) \left(\frac{MF_A(0)}{F_\pi} + \frac{g_{\pi NN} \Delta Q^2}{m_\pi^2} \right) + 2MF_A(Q^2) \right], \quad (16)$$

where $g_{\pi NN} = 13.21$, $F_\pi = 92.42$ MeV and $\Delta = 1 + \frac{MF_A(0)}{F_\pi g_{\pi NN}}$.

Pseudoscalar form factor using Chiral Perturbation Theory(ChPT) is given by [30, 31, 34, 35]

$$F_P(Q^2) = \frac{2Mg_{\pi NN}F_\pi}{m_\pi^2 + Q^2} + \frac{F_A(0)M^2r_A^2}{3} \quad (17)$$

where axial radius $r_A = \frac{2\sqrt{3}}{M_A}$.

The form factors $F_3^V(Q^2)$ and $F_3^A(Q^2)$ are associated with the second class current(SCC). There are no compelling reasons for their existence as they violate charge or time symmetry and in the case of $F_3^V(Q^2)$ also the conserved vector current. Almost all the current calculations of neutrino reactions assume SCC to be zero. However, there are some experimental analyses of semileptonic weak interactions like beta decays, muon capture and neutrino scattering in the $\Delta S = 0$ sector which give upper limits on these form factors which are consistent with the constraints of the present data on these processes [19, 66–68]. We have used the following expressions for $F_3^V(Q^2)$ as given in Ref. [66]

$$F_3^V(Q^2) = \frac{F_3^V(0)}{\left(1 + \frac{Q^2}{M_3^V}\right)^2}. \quad (18)$$

For our numerical calculations we have taken $F_3^V(0) = 1.6$ and $M_3^V = 1$ GeV [66]. Another expression for $F_3^V(Q^2)$ as given in Ref.[19] is

$$F_3^V(Q^2) = 4.4 F_1^V(Q^2). \quad (19)$$

The axial form factor associated with the second class current $F_3^A(Q^2)$ is taken as [19, 66]

$$F_3^A(Q^2) = 0.15 F_A(Q^2). \quad (20)$$

The parameterization of form factors discussed above will be used in the evaluation of the CCQE cross section. The differential scattering cross section for reaction given in Eq.(1) in the laboratory frame is in general written as,

$$d\sigma = \frac{(2\pi)^4 \delta^4(k + p - p' - k')}{4(k \cdot p)} \frac{d^3 \vec{k}'}{(2\pi)^3 2E_l} \frac{d^3 \vec{p}'}{(2\pi)^3 2E_p} |\mathcal{M}|^2. \quad (21)$$

The double differential cross section $\sigma_{free}(E_l, |\vec{k}'|)$ on free nucleon is then obtained as

$$\sigma_{free}(E_l, |\vec{k}'|) \equiv \frac{d^2 \sigma}{dE_l d|\vec{k}'|} = \frac{|\vec{k}'|^2}{4\pi E_\nu E_l} \frac{M^2}{E_n E_p} \bar{\Sigma} \Sigma |\mathcal{M}|^2 \delta[q_0 + E_n - E_p] \quad (22)$$

Inside the nucleus, the neutrino scatters from a neutron moving in a finite nucleus of neutron density $\rho_n(r)$, with a local occupation number $n_n(\vec{p}, \vec{r})$ of the initial nucleon of momentum \vec{p} localized in a region r , the radius of the nucleus. In the local density approximation the scattering cross section is written as

$$\sigma(E_l, |\vec{k}'|) = \int 2d\vec{r}d\vec{p} \frac{1}{(2\pi)^3} n_n(\vec{p}, \vec{r}) \sigma_{free}(E_l, |\vec{k}'|) \quad (23)$$

where $\sigma_{free}(E_l, |\vec{k}'|)$ is given by Eq.(22). The neutron energy E_n and proton energy E_p are replaced by $E_n(|\vec{p}|)$ and $E_p(|\vec{p} + \vec{q}|)$, where \vec{p} is now the momentum of the target nucleon inside the nucleus. This is because inside the nucleus the nucleons are not free and their momenta are constrained to satisfy the Pauli principle, i.e., $p < p_{F_n}$ and $p' = |\vec{p} + \vec{q}| > p_{F_p}$, where p_{F_n} and p_{F_p} are the local Fermi momenta of neutrons and protons at the interaction point in the nucleus and are given by $p_{F_n} = [3\pi^2 \rho_n(r)]^{\frac{1}{3}}$ and $p_{F_p} = [3\pi^2 \rho_p(r)]^{\frac{1}{3}}$, $\rho_n(r)$ and $\rho_p(r)$ are the neutron and proton nuclear densities which are given in terms of the nuclear density $\rho(r)$:

$$\rho_n(r) = \frac{(A - Z)}{A} \rho(r); \quad \rho_p(r) = \frac{Z}{A} \rho(r). \quad (24)$$

	c_1		c_2		Q -value		$B.E.$	p_F
	c_1^n	c_1^p	c_2^n	c_2^p	ν	$\bar{\nu}$	ν	$\bar{\nu}$
^{12}C	1.692	1.692	1.082*	1.082*	16.8	13.9	25	221 221
^{40}Ar	3.64	3.47	0.569	0.569	2.5	8.0	30	259 242
^{56}Fe	4.05	3.971	0.5935	0.5935	6.8	4.8	36	263 251
^{208}Pb	6.89	6.624	0.549	0.549	2.4	5.5	44	283 245

TABLE I: Different parameters used for numerical calculations for various nuclei. c_1 and c_2 are the density parameters(in Fermi units) defined for modified harmonic oscillator as $\rho(r) = \rho_0(1 + c_2(\frac{r}{c_1})^2)\exp(-(\frac{r}{c_1})^2)$ and for 2-parameter Fermi density as $\rho(r) = \rho_0/(1+\exp(\frac{r-c_1}{c_2}))$. For ^{12}C we have used modified harmonic oscillator density(* c_2 is dimensionless) and for ^{40}Ar , ^{56}Fe and ^{208}Pb nuclei, 2-parameter Fermi density have been used, where superscript n and p in density parameters($c_i^{n,p}$; $i=1,2$) stand for neutron and proton, respectively. The Q -value of the reaction, binding energy ($B.E.$) and Fermi momentum(p_F) for different nuclei are given in MeV.

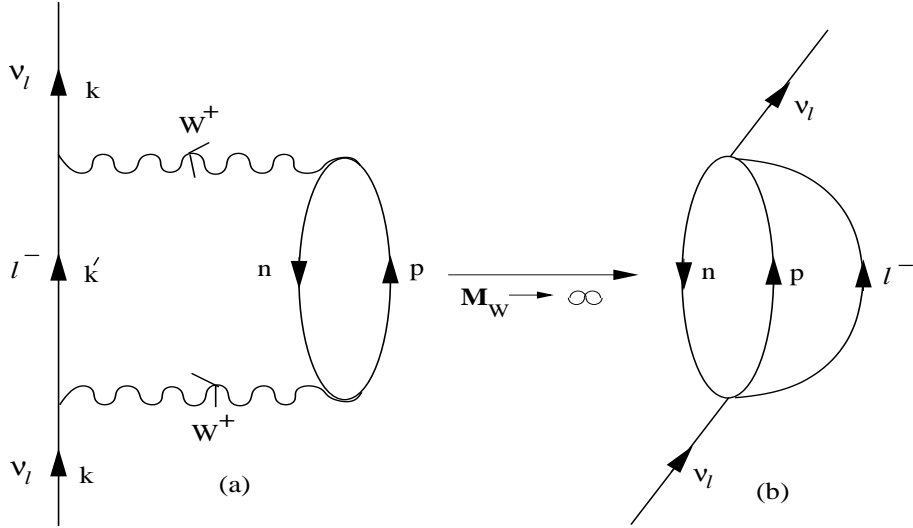


FIG. 1: Diagrammatic representation of the neutrino self-energy corresponding to the ph-excitation leading to $\nu_l + n \rightarrow l^- + p$ in nuclei. In the large mass limit of the intermediate vector boson(i.e. $M_W \rightarrow \infty$) the diagram (a) is reduced to (b) which is used to calculate $|\mathcal{M}|^2$ in Eq.(6).

The density parameters have been taken from Ref. [69, 70] and are summarized in Table I. For the antineutrino induced reaction on free nucleon or nucleons bound in a nucleus the role of neutron and proton get interchanged. Furthermore, in nuclei the threshold value of the reaction i.e. the Q -value of the reaction(Q_r) has to be taken into account, which we have taken to be the value corresponding to the lowest allowed Fermi transition or Gammow-Teller transition.

These considerations lead to a modification in the δ function used in Eq.(22) i.e. $\delta[q_0 + E_n - E_p]$ is modified to $\delta[q_0 + E_n(\vec{p}) - E_p(\vec{p} + \vec{q}) - Q_r]$ and the factor

$$\int \frac{d\vec{p}}{(2\pi)^3} n_n(\vec{p}, \vec{r}) \frac{M^2}{E_n E_p} \delta[q_0 + E_n - E_p] \quad (25)$$

occurring in Eq.(23) is replaced by $-(1/\pi)\text{Im}U_N(q_0, \vec{q})$, where $U_N(q_0, \vec{q})$ is the Lindhard function corresponding to the particle hole(ph) excitation [45] shown in Fig.(1) and is given by [45]:

$$U_N(q_0, \vec{q}) = \int \frac{d\vec{p}}{(2\pi)^3} \frac{M^2}{E_n E_p} \frac{n_n(p) [1 - n_p(\vec{p} + \vec{q})]}{q_0 + E_n(p) - E_p(\vec{p} + \vec{q}) + i\epsilon} \quad (26)$$

where $q_0 = E_\nu - E_l - Q_r$. For the antineutrino reaction the suffix n and p will get interchanged.

The imaginary part of the Lindhard function is obtained to be [45]:

$$ImU_N(q_0, \vec{q}) = -\frac{1}{2\pi} \frac{M^2}{|\vec{q}|} [E_{F_1} - A] \quad (27)$$

with $Q^2 > 0$, $E_{F_2} - q_0 < E_{F_1}$ and $\frac{-q_0 + |\vec{q}| \sqrt{1 + \frac{4M^2}{Q^2}}}{2} < E_{F_1}$, where $E_{F_1} = \sqrt{p_{F_n}^2 + M^2}$, $E_{F_2} = \sqrt{p_{F_p}^2 + M^2}$ and $A = \text{Max} \left[M, E_{F_2} - q_0, \frac{-q_0 + |\vec{q}| \sqrt{1 + \frac{4M^2}{Q^2}}}{2} \right]$.

With inclusion of these nuclear effects the cross section $\sigma(E_\nu)$ is written as

$$\begin{aligned} \sigma(E_\nu) = & -2G_F^2 \cos^2 \theta_c \int_{r_{min}}^{r_{max}} r^2 dr \int_{k'_{min}}^{k'_{max}} k' dk' \int_{Q_{min}^2}^{Q_{max}^2} dQ^2 \frac{1}{E_\nu^2 E_l} \\ & \times L_{\mu\nu} J^{\mu\nu} ImU_N[E_\nu - E_l - Q_r, \vec{q}]. \end{aligned} \quad (28)$$

The outgoing lepton when comes out of the nucleus, its energy and momentum are modified due to the Coulomb interaction. The Coulomb distortion effect on the outgoing lepton has been taken into account in an effective momentum approximation(MEMA) [45] in which the lepton momentum and energy are modified. In the local density approximation, the effective energy of the lepton in the Coulomb field of the final nucleus is given by [45, 71]:

$$E_{eff} = E_l + V_c(r),$$

where

$$V_c(r) = Z_f \alpha 4\pi \left(\frac{1}{r} \int_0^r \frac{\rho_p(r')}{Z_f} r'^2 dr' + \int_r^\infty \frac{\rho_p(r')}{Z_f} r' dr' \right) \quad (29)$$

with α as fine structure constant and Z_f as the charge of outgoing lepton, taken as -1 for neutrino and $+1$ for antineutrino. This leads to a change in the imaginary part of the Lindhard function occurring in Eq. (28)

$$ImU_N[E_\nu - E_l - Q_r, \vec{q}] \rightarrow ImU_N(E_\nu - E_l - Q_r - V_c(r), \vec{q})$$

Furthermore, in a nucleus the response of electroweak strength may change due to the presence of strongly interacting nucleons. These changes are calculated by considering the interaction of ph excitations in the nuclear medium in Random Phase Approximation (RPA) as shown in Fig.2. The diagram shown in Fig.2 simulates the effects of the strongly interacting nuclear medium at the weak vertex. The ph-ph interaction is shown by the wavy line in Fig.2 and is described by the π and ρ exchanges modulated by the effect of short range correlations. The effect of the Δ degrees of freedom in the nuclear medium is included in the calculation of the RPA response by considering the effect of ph- Δh and Δh - Δh excitations as shown in Fig.2(b). This is done by replacing U_N by $U_N = U_N + U_\Delta$, where U_Δ is the Lindhard function for Δh excitation in the nuclear medium and the expressions for U_N and U_Δ are taken from Ref. [72]. The different couplings of N and Δ are incorporated in U_N and U_Δ . The details of which are discussed in Refs. [44],[46]. In the appendix we have given the expression for the hadronic tensor in covariant form as well as the expression for the hadronic tensor when RPA corrections are incorporated. We must point out that the RPA corrections are implemented in the leading order terms only.

Thus, in a local density approximation in the presence of nuclear medium effect including the RPA effect, the total cross section $\sigma(E_\nu)$, is written as

$$\begin{aligned} \sigma(E_\nu) = & -2G_F^2 \cos^2 \theta_c \int_{r_{min}}^{r_{max}} r^2 dr \int_{k'_{min}}^{k'_{max}} k' dk' \int_{Q_{min}^2}^{Q_{max}^2} dQ^2 \frac{1}{E_\nu^2 E_l} L_{\mu\nu} J_{RPA}^{\mu\nu} \\ & \times ImU_N[E_\nu - E_l - Q_r - V_c(r), \vec{q}] \end{aligned} \quad (30)$$

where $J_{RPA}^{\mu\nu}$ is the modified hadronic tensor when RPA effect is incorporated. Explicit expression of $J_{RPA}^{\mu\nu}$ is given in the appendix.

Now we discuss in brief the form of the various other Fermi gas model used in literature [42, 43]. In the Llewellyn Smith Fermi gas model [42] the cross section per nucleon in a nucleus is equal to the cross section for a free nucleon i.e. σ_{free} defined in Eq.22, multiplied by $[1 - \frac{D}{N}]$, where

$$\begin{aligned} D &= Z \text{ for } 2x < u - v \\ &= \frac{1}{2} A \left\{ 1 - \frac{3x}{4}(u^2 + v^2) + \frac{x^3}{2} - \frac{3}{32x}(u^2 - v^2)^2 \right\} \text{ for } u - v < x < u + v \\ &= 0 \text{ for } x > u + v \end{aligned} \quad (31)$$

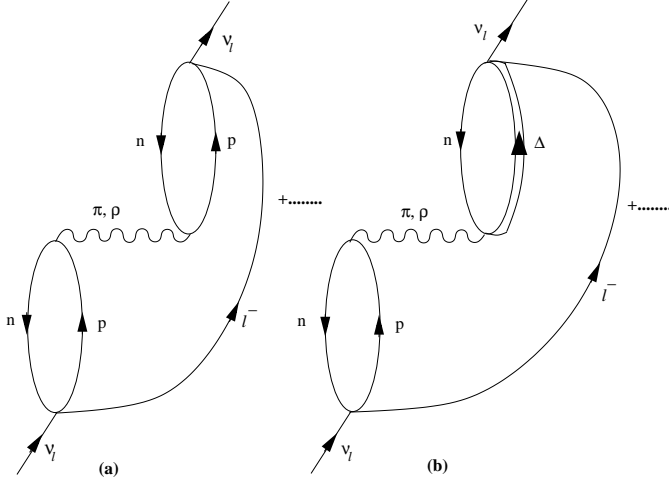


FIG. 2: Many body Feynman diagrams (drawn in the limit $M_W \rightarrow \infty$) accounting for the medium polarization effects contributing to the process $\nu_l + n \rightarrow l^- + p$.

with $x = \frac{|\vec{q}|}{2p_F}$, $u = (\frac{2N}{A})^{1/3}$, $v = (\frac{2Z}{A})^{1/3}$ and $N (= A - Z)$, Z , A are neutron, proton and mass numbers of the initial nucleus respectively, p_F is the Fermi momentum and the three momentum transfer $|\vec{q}| = \sqrt{q_0^2 + Q^2}$.

Smith and Moniz [41] used the following expression for the double differential cross section in the Fermi gas model:

$$\begin{aligned} \frac{d^2\sigma}{dk'd\Omega_l} &= \frac{G_F^2 k'^2 \cos^2(\frac{1}{2}\chi)}{2\pi^2 M} \left\{ W_2 + [2W_1 + \frac{m_l^2}{M^2} W_\alpha] \tan^2(\frac{1}{2}\chi) \right. \\ &+ (W_\beta + W_8) m_l^2 / (M E_l \cos^2(\frac{1}{2}\chi)) - 2W_8/M \tan(\frac{1}{2}\chi) \\ &\times \left. \sec(\frac{1}{2}\chi) [-Q^2 \cos^2(\frac{1}{2}\chi) + |\vec{q}|^2 \sin^2(\frac{1}{2}\chi) + m_l^2]^{\frac{1}{2}} \right\}, \end{aligned} \quad (32)$$

where $\cos \chi = \frac{k'}{E_l} \cos \theta$. The form of W_i 's and other details are given in Ref. [41].

Gaisser and O'Connell [43] have used relativistic response function $R(q, q_0)$, in a Fermi gas model to take into account nuclear medium effects, the expression for the double differential scattering cross section is given by

$$\begin{aligned} \frac{d^2\sigma}{d\Omega_l dE_l} &= C \frac{d\sigma_{free}}{d\Omega_l} R(q, q_0), \\ R(q, q_0) &= \frac{1}{\frac{4}{3}\pi p_{F_N}^3} \int \frac{d^3p_N}{E_N E_{N'}} \frac{M^2}{\delta(E_N + q_0 - E_B - E_{N'})} \delta(p_{F_N} - |\vec{p}_N|) \theta(|\vec{p}_N + \vec{q}| - p_{F_{N'}}), \end{aligned} \quad (33)$$

where p_{F_N} is the Fermi momentum for the initial nucleon, $N, N' = n$ or p and $C = A - Z$ for neutrino induced process and $C = Z$ for the antineutrino induced process. $\frac{d\sigma_{free}}{d\Omega_l}$ is the differential scattering cross section for the (anti)neutrino reaction on free (proton)neutron target and we have used the same expression for the form factors as used in the Local Fermi Gas Model for the numerical calculations. Different parameters associated with nuclear densities, Q -value of the reaction, binding energy and Fermi momentum used in the numerical calculations are summarized in Table-I.

III. RESULTS AND DISCUSSION

A. Nuclear model dependence

In this section, we present the results and discuss the findings. In Fig. 3, the results are presented for the ratio of scattering cross section per interacting nucleon to the scattering cross section on free nucleon target for (anti)neutrino induced processes in ^{12}C , ^{40}Ar , ^{56}Fe and ^{208}Pb in the energy region from threshold to 0.8 GeV. The results are obtained using Local Fermi Gas Model(LFG) i.e. the expression given in Eq.28 and the Local Fermi Gas Model

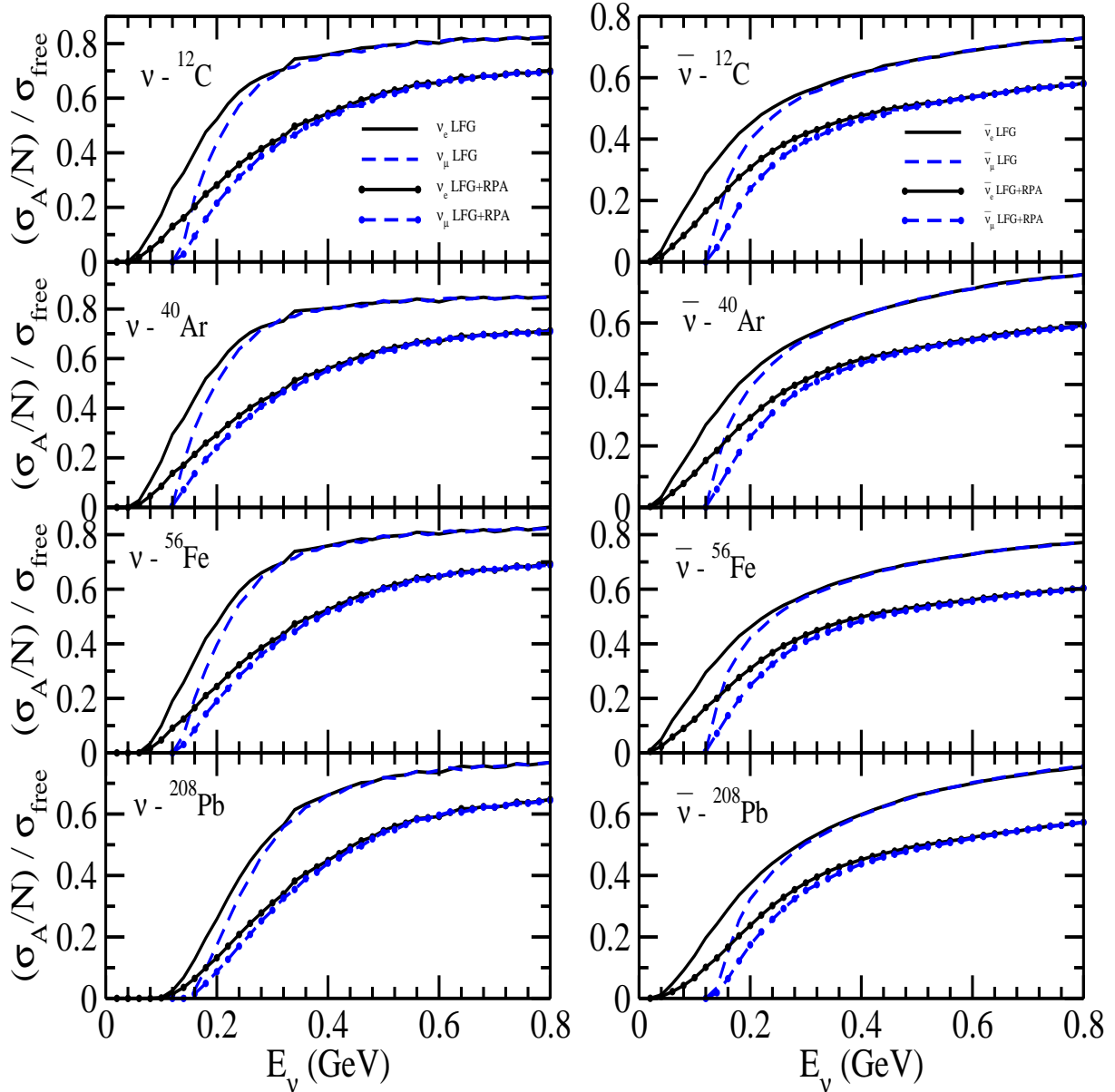


FIG. 3: Ratio $\frac{\sigma_A/N}{\sigma_{\text{free}}}$ vs E_ν , for neutrino(Left panel) and antineutrino(Right panel) induced processes in ^{12}C , ^{40}Ar , ^{56}Fe and ^{208}Pb . The solid(dashed) line represent cross section obtained from electron(muon) type neutrino and antineutrino beams. For neutrino induced process $N = A - Z$, is neutron number and for antineutrino induced process $N = Z$, is proton number. σ_A is cross section in nuclear target and has been evaluated using Local Fermi Gas Model(LFG) and LFG with RPA effect(LFG+RPA) and σ_{free} is the cross section for the free nucleon case.

with RPA effect(LFG+RPA) i.e. using Eq.30 to the cross section obtained for the free nucleon case using Eq.21 on neutron(proton) target induced by neutrino(antineutrino).

Performing calculations using LFG, we find that in ^{12}C the nuclear medium effects like Fermi motion, Pauli blocking, binding energy, the cross section reduces by $\sim 30\%(42\%)$ at $E_\nu = 0.3$ GeV and around $20(30)\%$ at $E_\nu = 0.6$ GeV from free nucleon case for $\nu_e(\bar{\nu}_e)$ induced processes. Inclusion of RPA correlation in LFG, reduces the cross section for $\nu_e(\bar{\nu}_e)$ scattering from free nucleon by $\sim 55\%(56\%)$ at $E_\nu = 0.3$ GeV and $35\%(45\%)$ at $E_\nu = 0.6$ GeV. Similar results may be observed for ^{40}Ar , ^{56}Fe and ^{208}Pb nuclear targets. In general the reduction in the cross section increases with the increase in mass number. For ν_μ and $\bar{\nu}_\mu$ induced processes at lower energies the reduction is larger and for $E_\nu > 0.4$ GeV, the reduction in $\nu_e(\bar{\nu}_e)$ and $\nu_\mu(\bar{\nu}_\mu)$ cross sections is almost the same. This will be discussed separately in the next section when we compare electron and muon scattering cross sections.

To compare our results with other variants of Fermi gas model, we have obtained total scattering cross section

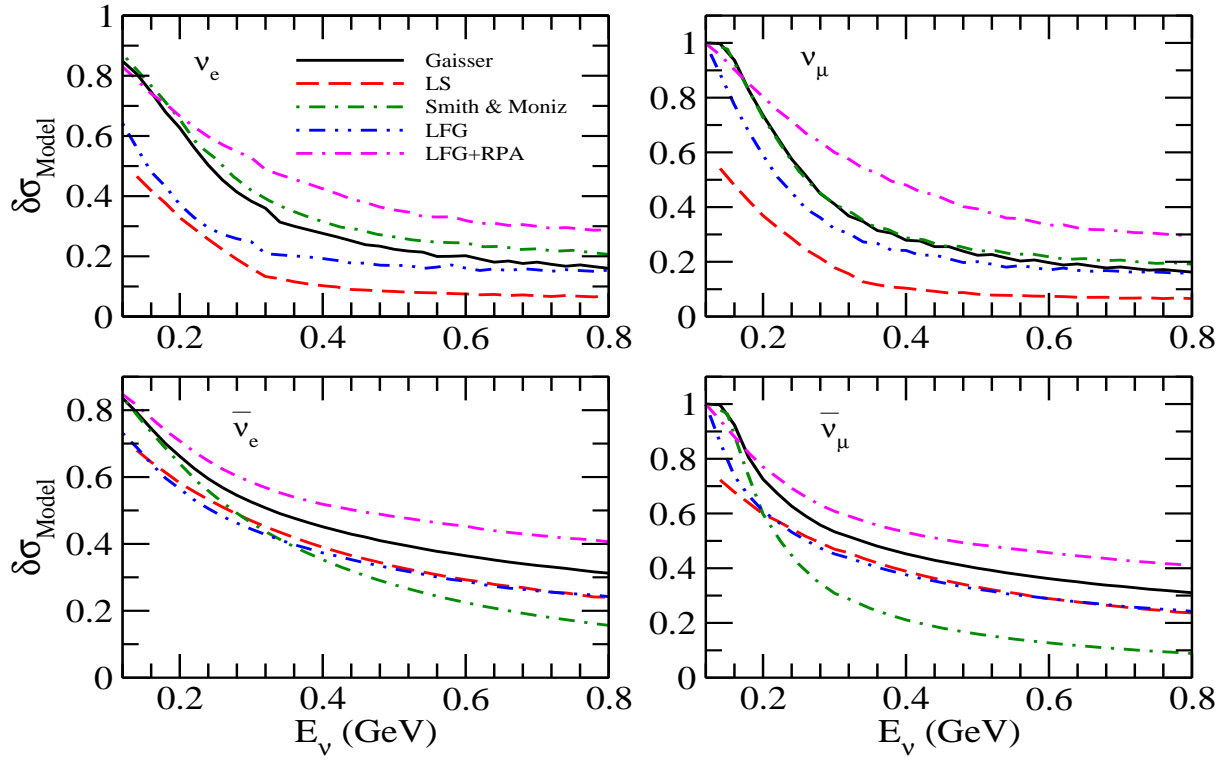


FIG. 4: The fractional suppression in cross section $\delta\sigma_{\text{Model}} = \frac{\sigma_{\text{free}} - \sigma_{\text{Model}}}{\sigma_{\text{free}}}$ vs E_ν , where σ_{free} is the cross section obtained for free nucleon and σ_{Model} is per interacting nucleon cross section in ^{40}Ar obtained by using different nuclear models. The results are presented for the cross sections obtained from different models of Fermi gas(σ_{Model}) viz. Gaisser O' Connell(solid line), Llewellyn Smith(dashed line), Smith and Moniz(dashed dotted line) and with(double dashed dotted line) & without RPA(dashed double dotted line) effect using Local Fermi Gas Model. The top panel is for neutrino and bottom panel is for antineutrino induced processes.

in ^{40}Ar using Fermi gas model of Smith and Moniz [41], Llewellyn Smith [42], and Gaisser and O'Connell [43] and calculated fractional difference $\delta\sigma_{\text{Model}} = \frac{\sigma_{\text{free}} - \sigma_{\text{Model}}}{\sigma_{\text{free}}}$, the results for which are shown in Fig.4. Here σ_{free} stands for the (anti)neutrino induced interaction cross section on free nucleon target and σ_{Model} stands for the (anti)neutrino induced interaction cross section for the nucleons bound inside the nucleus. We find appreciable difference in the results when various nuclear models are used. For example, when calculations are performed by using Fermi gas model of Llewellyn Smith [42], the cross sections get reduced from the free nucleon case by $\sim 16\%(\sim 45\%)$ at $E_\nu = 0.3 \text{ GeV}$ and around $8\%(\sim 30\%)$ at $E_\nu = 0.6 \text{ GeV}$ for $\nu_e(\bar{\nu}_e)$ induced scattering processes. While when one uses Fermi gas model of Smith and Moniz [41] this reduction in the cross section from the free nucleon case is $\sim 42\%(\sim 45\%)$ at $E_\nu = 0.3 \text{ GeV}$ and $\sim 24\%(\sim 22\%)$ at $E_\nu = 0.6 \text{ GeV}$. When the calculations are performed using Fermi gas model of Gaisser and O' Connell [43] the reduction from the free nucleon case is $\sim 38\%(\sim 52\%)$ at $E_\nu = 0.3 \text{ GeV}$ which becomes $20\%(35\%)$ at $E_\nu = 0.6 \text{ GeV}$ for $\nu_e(\bar{\nu}_e)$ induced processes. Performing calculations in the Local Fermi Gas Model, reduces the cross sections by $\sim 25\%(44\%)$ at $E_\nu = 0.3 \text{ GeV}$ and around $15(30)\%$ at $E_\nu = 0.6 \text{ GeV}$ for $\nu_e(\bar{\nu}_e)$ induced processes. Including RPA correlation with LFG, reduces the cross section by $\sim 54\%(58\%)$ at $E_\nu = 0.3 \text{ GeV}$ and $32\%(45\%)$ at $E_\nu = 0.6 \text{ GeV}$. The nuclear model dependence is found to be larger in the case of $\nu_\mu(\bar{\nu}_\mu)$ scattering than in the case of $\nu_e(\bar{\nu}_e)$ scattering in the energy region of $E_\nu < 0.8 \text{ GeV}$.

For $\nu_\mu(\bar{\nu}_\mu)$ induced scattering processes, reduction in the cross section from the free nucleon case is $\sim 18\%(47\%)$ at $E_\nu = 0.3 \text{ GeV}$ and $\sim 7\%(30\%)$ at $E_\nu = 0.6 \text{ GeV}$, when cross sections are obtained using Fermi gas model of Llewellyn Smith [42]. Fermi gas model of Smith and Moniz [41] reduces the cross section from the free nucleon case by $\sim 40\%(\sim 30\%)$ at $E_\nu = 0.3 \text{ GeV}$ and around $22\%(\sim 12\%)$ at $E_\nu = 0.6 \text{ GeV}$. When calculations are performed by using Fermi gas model of Gaisser and O' Connell [43] the reduction from the free nucleon case is $\sim 40\%(\sim 52\%)$ at $E_\nu = 0.3 \text{ GeV}$ which becomes $20\%(35\%)$ at $E_\nu = 0.6 \text{ GeV}$. The calculations are also performed in the Local Fermi Gas Model and we find that the cross sections get reduced by $\sim 26\%(45\%)$ at $E_\nu = 0.3 \text{ GeV}$ and around $15\%(30\%)$ at $E_\nu = 0.6 \text{ GeV}$ for $\nu_\mu(\bar{\nu}_\mu)$ induced processes. Inclusion of RPA correlation with LFG, reduces the cross section for ν_μ scattering from free nucleon value by $\sim 58\%$ at $E_\nu = 0.3 \text{ GeV}$ and 32% at $E_\nu = 0.6 \text{ GeV}$, which for $\bar{\nu}_\mu$ induced

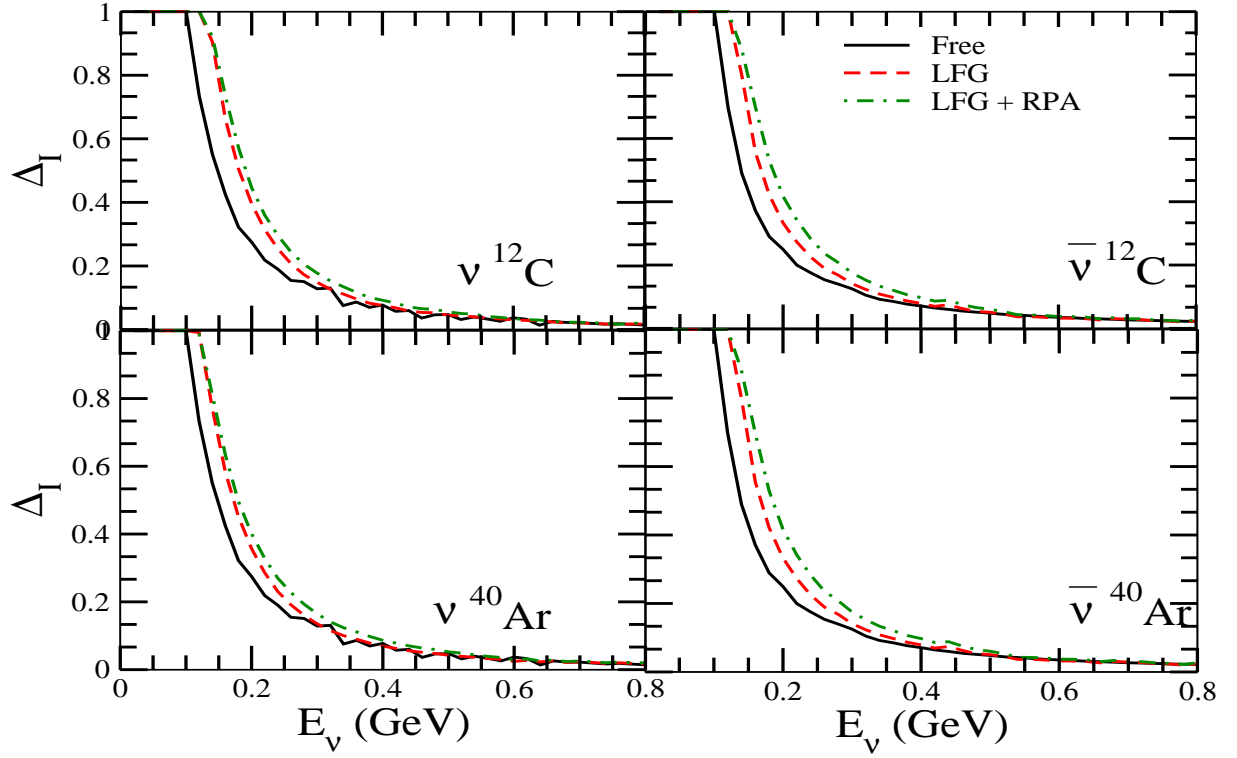


FIG. 5: $\Delta_I = \frac{\sigma_{\nu_e(\bar{\nu}_e)} - \sigma_{\nu_\mu(\bar{\nu}_\mu)}}{\sigma_{\nu_e(\bar{\nu}_e)}}$ for neutrino(left panel) and antineutrino(right panel) induced processes in ^{12}C and ^{40}Ar targets. Here I stands for the results of the cross sections obtained (i) for the free nucleon case(solid line) (ii) in the Local Fermi Gas Model(dashed line) and (iii) LFG with RPA effect(dashed dotted line).

scattering is $\sim 60\%$ at $E_\nu = 0.3$ GeV and $\sim 45\%$ at $E_\nu = 0.6$ GeV.

B. Effect of lepton mass and its kinematical implications

There are two types of corrections which appear when lepton mass m_l ($l = e, \mu$) is taken into account in the cross section calculations for the reaction $\nu_l(\bar{\nu}_l) + N \rightarrow l^-(l^+) + N'$, ($N, N' = n, p$) which can be classified as kinematical and dynamical in origin. The kinematical effects arise due to $E_l \neq |\mathbf{p}_l|$ in presence of m_l and the maximum and minimum values of four momentum transfer square ($Q^2 = -q^2 \geq 0$) i.e. Q_{max}^2 and Q_{min}^2 are modified affecting the calculations of total cross sections. These effects are negligible for highly relativistic leptons but could become important at low energies near threshold specially for muons. On the other hand, the dynamical corrections arise as additional terms proportional to $\frac{m_l^2}{M^2}$ in the existing contribution of vector and axial vector form factors as well as new contributions due to induced pseudoscalar and other form factors associated with the second class currents come into play. In fact all the contributions from the pseudoscalar form factor $F_P(Q^2)$ and the second class vector form factor $F_3^V(Q^2)$ are proportional to $\frac{m_l^2}{M^2}$ while the contribution from the second class axial vector form factor $F_3^A(Q^2)$ is proportional either to $\frac{m_l^2}{M^2}$ or $\frac{Q^2}{M^2}$ or both.

To study the lepton mass dependence on $\nu_e(\bar{\nu}_e)$ and $\nu_\mu(\bar{\nu}_\mu)$ induced scattering cross sections in free nucleon as well as in nuclear targets we define $\Delta_I = \frac{\sigma_{\nu_e(\bar{\nu}_e)} - \sigma_{\nu_\mu(\bar{\nu}_\mu)}}{\sigma_{\nu_e(\bar{\nu}_e)}}$ for neutrino(antineutrino) induced reactions in ^{12}C and ^{40}Ar nuclear targets, where $I = i, ii, iii$, which respectively stands for the cross sections obtained in (i) free neutrino/antineutrino-nucleon case, (ii) the Local Fermi Gas Model(LFG) and (iii) the Local Fermi Gas Model with RPA effect(LFG+RPA).

The results are presented in Fig.5, which show that the differences in the electron and muon production cross sections for $\nu(\bar{\nu})$ induced reactions on ^{12}C target are appreciable at low energies $E_\nu < 0.4$ GeV. For example, this fractional change is about 27%(25%) at $E_\nu = 0.2$ GeV and reduces to $\sim 8\%(7\%)$ at $E_\nu = 0.4$ GeV in the case of free nucleon. While in ^{12}C , using LFG it is approximately 40%(33%) at $E_\nu = 0.2$ GeV and $\sim 8\%$ for both neutrino and antineutrino at 0.4 GeV, respectively. However, using RPA effect with LFG, the difference is around 44%(42%) and

$\sim 9\%(10\%)$ at $E_\nu = 0.2 \text{ GeV}$ and 0.4 GeV , respectively.

While for the case of neutrino(antineutrino) induced process on ^{40}Ar target using LFG, this fractional change is approximately $35\%(33\%)$ and $\sim 7\%(8\%)$ at $E_\nu = 0.2 \text{ GeV}$ and 0.4 GeV , respectively. However, using RPA effect with LFG, the difference is around $40\%(42\%)$ and $\sim 9\%(10\%)$ at $E_\nu = 0.2 \text{ GeV}$ and 0.4 GeV , respectively.

C. Form factor dependence

The hadronic current defined in Eq.5 consists of six form factors; three isovector($F_i^V(Q^2), i = 1, 3$) and three axial vector($F_i^A(Q^2), i = 1, 3$) form factors. Among them, $F_i^V(Q^2), i = 1, 2$, are parameterized in terms of Sach's form factors $G_E^{p,n}(Q^2)$ and $G_M^{p,n}(Q^2)$. Various parameterization for $G_E^{p,n}(Q^2)$ and $G_M^{p,n}(Q^2)$ are available in literature [65, 73], however, different choices do not change neutrino-nucleus cross section by more than a percent. $F_3^V(Q^2)$, which arises due to the second class current is generally ignored in calculations. Similarly, the axial current consists of three form factors viz. $F_A(Q^2)$, $F_P(Q^2)$ and $F_A^3(Q^2)$, among them $F_A(Q^2)$ is dominant and is parameterized in a dipole form with axial dipole mass(M_A). Unlike the small dependence on the choice of $G_E^{p,n}(Q^2)$ and $G_M^{p,n}(Q^2)$ on cross section, the cross section shows a strong dependence on the choice of M_A . The world average(WA) value of M_A is 1.026 GeV [30]. However, recently experiments like MINERvA [20], K2K [74], T2K [75], SciBooNE [27], MiniBooNE [23] have reported different values for M_A , like 0.99 GeV , 1.20 GeV , 1.26 GeV , 1.3 GeV and 1.39 GeV , respectively. This uncertainty in the choice of M_A affects the cross section which is discussed below.

1. Axial vector form factor

To show the explicit dependence of cross sections on axial dipole mass for neutrino/antineutrino scattering processes, we have changed M_A from the base value (taken as the world average value) and obtained the results for δ_{M_A} defined below in Eq. 34 and Δ_{M_A} defined in Eq. 35 by taking the two different values of M_A as 0.9 GeV and 1.2 GeV . These results are obtained for the (anti)neutrino induced processes on free nucleon as well as in the LFG with and without RPA effect for ^{40}Ar nuclear target.

The dependence on axial dipole mass is shown in Fig.6, by defining δ_{M_A} as

$$\delta_{M_A} = \frac{\sigma_{\nu_l}(M_A^{\text{modified}}) - \sigma_{\nu_l}(M_A = WA)}{\sigma_{\nu_l}(M_A = WA)}, \quad WA = 1.026 \text{ GeV} \quad (34)$$

where $l = e$ or $l = \mu$. We observe from Fig.6 that for free nucleon when a modified value of M_A i.e. $M_A^{\text{modified}} = 0.9(1.2) \text{ GeV}$ is used instead of world average value of 1.026 GeV then a decrease(increase) of $5 - 15\%$ is obtained for ν_e/ν_μ reactions in the energy range of 0.2 GeV to 0.8 GeV . In the case of $\bar{\nu}_e/\bar{\nu}_\mu$ -nucleon reactions this decrease(increase) is about $5 - 10\%$ in the same energy range. When nuclear medium effects are taken into account, for example, in the case of ^{40}Ar nucleus this decrease(increase) remains almost same. Therefore, the uncertainty in the (anti)neutrino-nucleus cross sections is the same as in the case of free (anti)neutrino-nucleon scattering processes.

We now study the sensitivity of the difference in electron and muon production cross sections due to the uncertainty in the choice of M_A . For this we define

$$\begin{aligned} \Delta_1(E_\nu) &= \frac{\sigma_{\nu_\mu}(M_A^{\text{modified}}) - \sigma_{\nu_e}(M_A^{\text{modified}})}{\sigma_{\nu_e}(M_A^{\text{modified}})}, \\ \Delta_2(E_\nu) &= \frac{\sigma_{\nu_\mu}(M_A = WA) - \sigma_{\nu_e}(M_A = WA)}{\sigma_{\nu_e}(M_A = WA)}, \\ \Delta_{M_A} &= \Delta_1(E_\nu) - \Delta_2(E_\nu). \end{aligned} \quad (35)$$

and show the numerical values for Δ_{M_A} for free nucleon and nuclei in Fig. 7. We observe that for free nucleon some sensitivity to the difference in the electron and muon production cross sections exists at low energies $E_\nu < 0.4 \text{ GeV}$ which does not exceed 1% . In nuclear target, when nuclear medium effects are taken into account this sensitivity remains almost the same as in the case of free neutrino-nucleon scattering process. Similar effects are found for the case of antineutrino induced reactions.

From Figs. 6 and 7, it may be observed that the cross section is very sensitive to the choice of axial dipole mass M_A . Therefore, while calculating the charged lepton production cross sections, the value of M_A should be carefully taken.

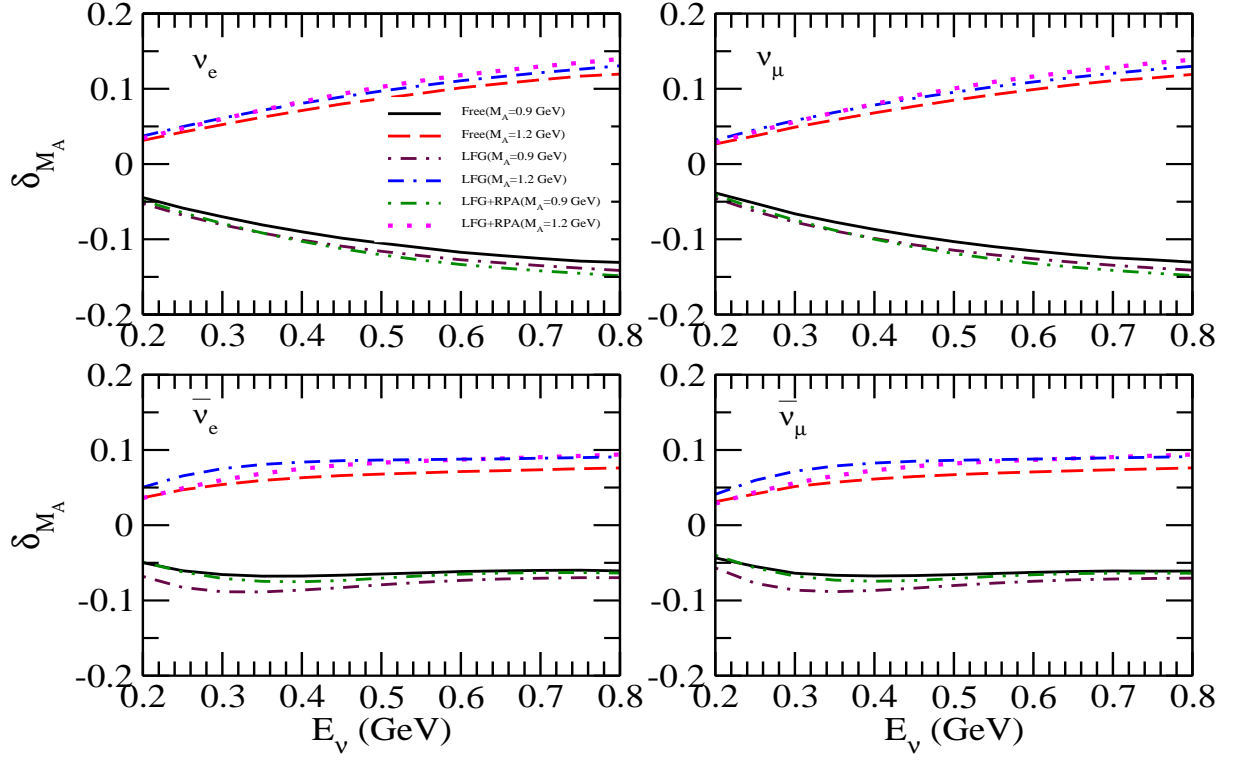


FIG. 6: The dependence of cross section on M_A obtained using Eq. 34. The results are shown for $\nu_e(\bar{\nu}_e)$ and $\nu_\mu(\bar{\nu}_\mu)$ induced processes on free nucleon as well as on ^{40}Ar target using LFG with and without RPA effect. Solid(dashed) line denotes results for the free nucleon case with $M_A = 0.9$ GeV(1.2 GeV), results obtained using LFG are shown by dashed dotted(double dashed dotted) with $M_A = 0.9$ GeV(1.2 GeV) and results for LFG with RPA effect are shown by dashed double dotted(dotted) with $M_A = 0.9$ GeV(1.2 GeV).

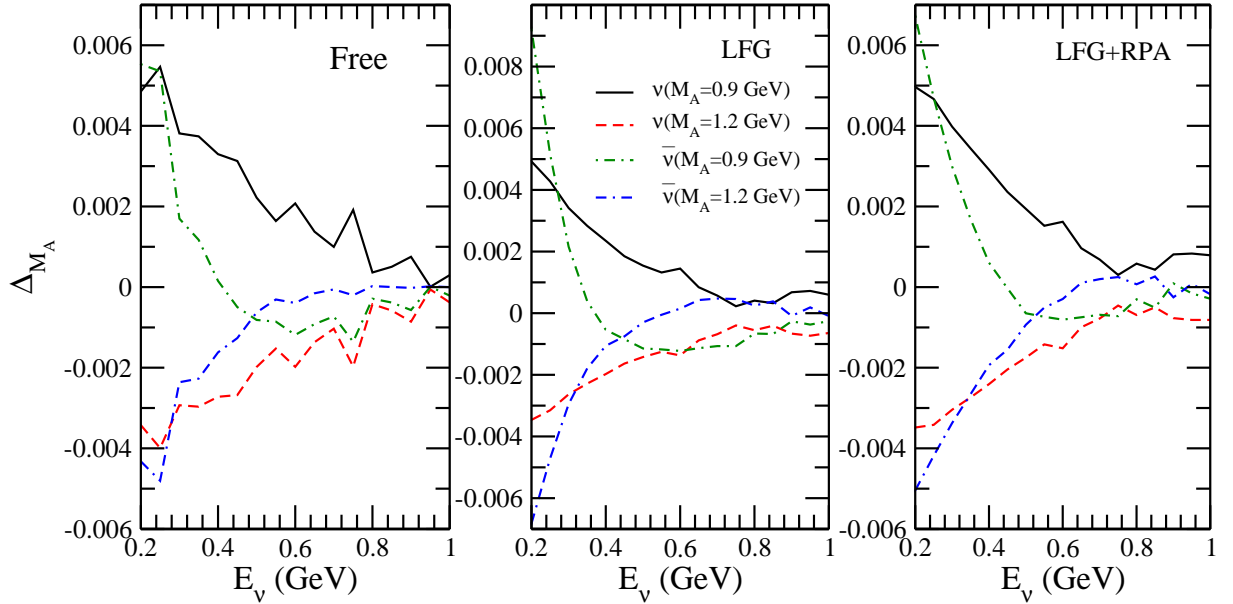


FIG. 7: Effect of axial dipole mass on the cross section (from left to right): on free nucleon; LFG, with and without RPA effect on ^{40}Ar target. Here different values of M_A are taken such as 0.9 GeV and 1.2 GeV. The fractional difference(Eq. 35) has been obtained using the base value of M_A taken as the world average value. Solid(dashed) line denotes results for the neutrino induced processes while for antineutrino the results are shown by dashed dotted(double dashed dotted) with $M_A = 0.9$ GeV(1.2 GeV).

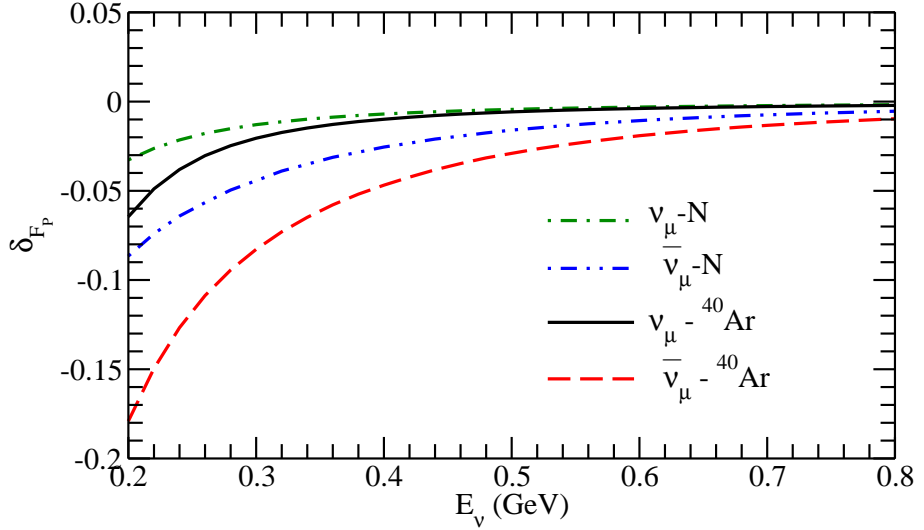


FIG. 8: Results of the fractional change δ_{F_P} defined in Eq.36 as a function of (anti)neutrino energy. The results are shown for the ν_μ induced interaction cross section for the free nucleon case(dashed dotted line), as well as for the nucleons bound in ^{40}Ar (solid line) nuclear target obtained by using LFG with RPA effect. The results corresponding to $\bar{\nu}_\mu$ induced CCQE process are shown by dashed double dotted line (free nucleon case) and dashed line(^{40}Ar target).

2. Pseudoscalar form factor

To study the effect of pseudoscalar form factor $F_P(Q^2)$ on muon production cross sections, we define

$$\delta_{F_P}(E_\nu) = \frac{\sigma_{\nu\mu}(F_P \neq 0) - \sigma_{\nu\mu}(F_P = 0)}{\sigma_{\nu\mu}(F_P = 0)}, \quad (36)$$

and similar expression for antineutrino is used. For the numerical calculations expression of $F_P(Q^2)$ given in Eq. 15 has been used. The results are presented in Fig.8. We find that δ_{F_P} is more sensitive in the case of $\bar{\nu}_\mu$ induced CCQE process than ν_μ induced process for the free nucleon case as well as for ^{40}Ar nuclear target. This sensitivity decreases with the increase in $\nu_\mu/\bar{\nu}_\mu$ energy and almost vanishes beyond 0.6 GeV .¹

We also study the sensitivity of pseudoscalar form factor $F_P(Q^2)$ to find out the difference in the electron vs muon production cross sections that are obtained using Eq.15. For this we define

$$\Delta_1(E_\nu) = \frac{\sigma_{\nu\mu}(F_P \neq 0) - \sigma_{\nu e}(F_P \neq 0)}{\sigma_{\nu e}(F_P \neq 0)}, \quad (37)$$

$$\Delta_2(E_\nu) = \frac{\sigma_{\nu\mu}(F_P = 0) - \sigma_{\nu e}(F_P = 0)}{\sigma_{\nu e}(F_P = 0)}, \quad (38)$$

$$\Delta_{F_P} = \Delta_1(E_\nu) - \Delta_2(E_\nu). \quad (39)$$

and the results for Δ_{F_P} are shown in Fig. 9. Similar expressions are also used for antineutrino induced processes.

We have calculated the fractional difference Δ_{F_P} as given in Eq. 39 for free nucleon case as well as for nucleons bound in ^{40}Ar nuclear target using the Local Fermi Gas Model with RPA effect. We observe that the inclusion of pseudoscalar form factor decreases the fractional change(Δ_{F_P}) by about 3%(8%) at $E_{\nu(\bar{\nu})} \sim 0.2\text{GeV}$ and becomes smaller with the increase in energy. When the nuclear medium effects(LFG+RPA) are taken into account in the evaluation of cross sections in ^{40}Ar then this difference increases to 4%(15%) at the same energy for neutrino(antineutrino) induced processes.

¹ Using the three different expressions of the pseudoscalar form factor $F_P(Q^2)$ given in Eqs. 15, 16 and 17, we have studied the behavior of $F_P(Q^2)$ vs Q^2 and found hardly any difference in the Q^2 dependence and therefore the total scattering cross section σ for ν_μ and $\bar{\nu}_\mu$ induced processes are also unaffected by the choice of $F_P(Q^2)$.

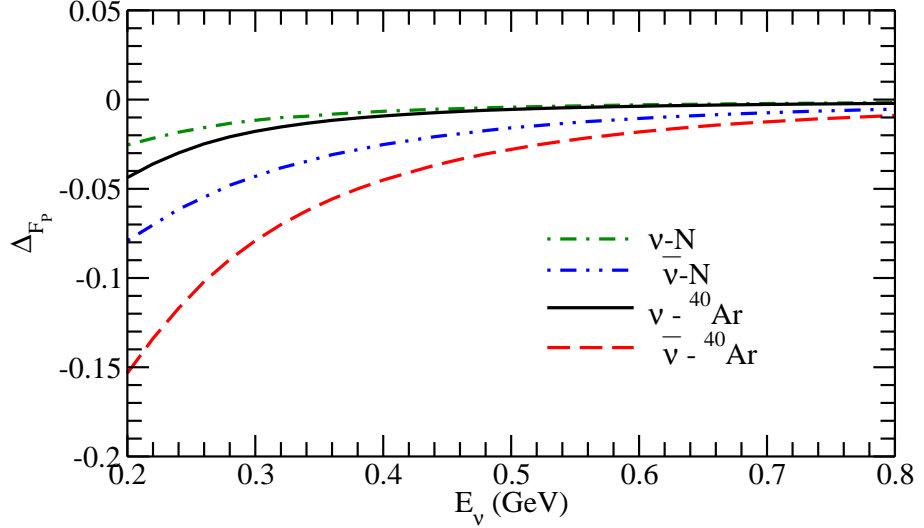


FIG. 9: Results of the fractional change Δ_{F_p} defined in Eq.39 as a function of (anti)neutrino energy. The results are shown for the neutrino induced interaction cross section for the free nucleon case(dashed dotted line), as well as for the nucleons bound in ^{40}Ar (solid line) nuclear target obtained by using LFG with RPA effect. The results corresponding to antineutrino induced CCQE process are shown by dashed double dotted line(free nucleon case) and dashed line(^{40}Ar target).

D. Second class currents

We have also studied the effect of second class current, due to which two additional form factors viz. F_3^V and F_3^A are introduced.

1. Second class vector current

The contribution of the second class vector form factor $F_3^V(Q^2)$ to the cross section is always proportional to the mass of the lepton so it is quite small in the case of $\nu_e(\bar{\nu}_e)$ as compared to $\nu_\mu(\bar{\nu}_\mu)$ reactions on nucleons and nuclei. We first study the overall contribution made by the second class vector form factor $F_3^V(Q^2)$ to the cross section in the case of muon neutrinos and define

$$\delta_{F_3^V}(E_\nu) = \frac{\sigma_{\nu\mu}(F_3^V \neq 0) - \sigma_{\nu\mu}(F_3^V = 0)}{\sigma_{\nu\mu}(F_3^V = 0)}, \quad (40)$$

Similar expression is used for antineutrino. For the numerical calculations we use Eq. 18 [66], and the results are shown in Fig.10. We find that the contribution of $F_3^V(Q^2)$ to the cross section is very small for ν_μ scattering on nucleons and nuclei. In the case of $\bar{\nu}_\mu$ scattering on nucleons at low energy, the contribution of $F_3^V(Q^2)$ at $E_{\nu/\bar{\nu}} = 0.2$ GeV is 5% which increases to 7% in ^{40}Ar when nuclear medium effects are taken into account.

We now study the sensitivity due to $F_3^V(Q^2)$ in the difference between the electron and muon production cross sections for free nucleon and nuclei. Sensitivity that arises in electron and muon production cross sections due to the presence of $F_3^V(Q^2)$ is studied by defining

$$\Delta_1(E_\nu) = \frac{\sigma_{\nu\mu}(F_3^V \neq 0) - \sigma_{\nu e}(F_3^V \neq 0)}{\sigma_{\nu e}(F_3^V \neq 0)} \quad (41)$$

$$\Delta_2(E_\nu) = \frac{\sigma_{\nu\mu}(F_3^V = 0) - \sigma_{\nu e}(F_3^V = 0)}{\sigma_{\nu e}(F_3^V = 0)} \quad (42)$$

$$\Delta_{F_3^V} = \Delta_1(E_\nu) - \Delta_2(E_\nu), \quad (43)$$

For the numerical calculations we have used the form of $F_3^V(Q^2)$ given in Eq.18 [66]. First, we present the results for $\Delta_1(E_\nu)$ as a function of neutrino/antineutrino energies and the results are shown in Fig. 11. These results are

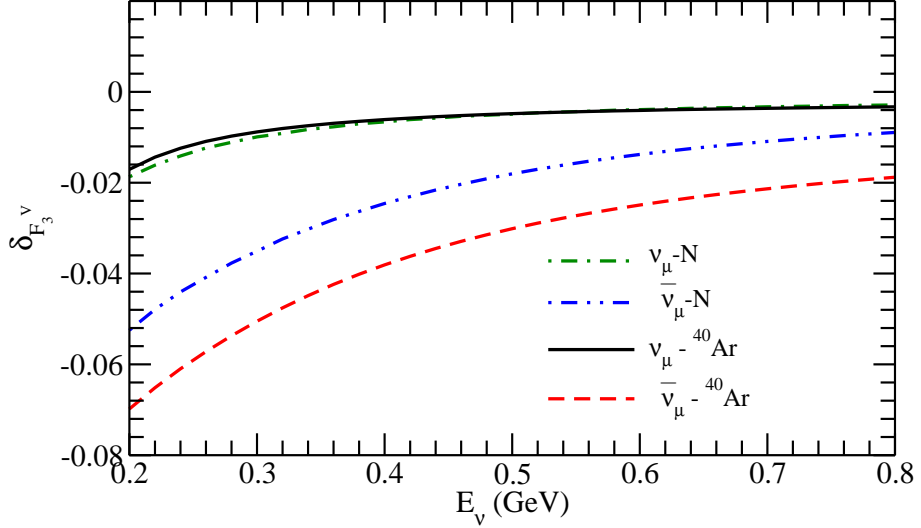


FIG. 10: Results of the fractional change $\delta_{F_3^V}$ defined in Eq.40 as a function of (anti)neutrino energy. The results are shown for ν_μ induced interaction cross section for the free nucleon case(dashed dotted line), as well as for the nucleons bound in ^{40}Ar (solid line) nuclear target obtained by using LFG. The results corresponding to $\bar{\nu}_\mu$ induced CCQE process are shown by dashed double dotted line(free nucleon case) and dashed line(^{40}Ar target).

presented for the free nucleon case as well as bound nucleons in ^{40}Ar , and the cross sections are obtained using the expression of the hadronic current with second class vector current. We must point out that the contribution from the second class axial current is switched off. We find that $\Delta_1(E_\nu)$ is sensitive to the flavor of neutrinos especially at low energies ($E_{\nu/\bar{\nu}} < 0.3\text{GeV}$) which is mainly due to threshold effect. Results of $\Delta_1(E_\nu)$ changes in nuclear targets when some nuclear model is used like LFG. However, it is not sensitive to the choice of nuclear model.

In Fig. 12, we present the results for $\Delta_{F_3^V}$ using Eq. 43 and obtained it for the free nucleon case as well as for ^{12}C and ^{40}Ar nuclear targets. We find that the effects are energy dependent and are more pronounced at low energies. From the figure it may be noticed that the fractional change is the same for both ^{12}C and ^{40}Ar nuclei. For example, for the case of neutrino, at $E_\nu = 0.2\text{ GeV}$, $\Delta_{F_3^V}$ is $\sim 1\%$ for free nucleon as well as in ^{40}Ar evaluated using LFG and the difference becomes almost negligible beyond $E_\nu = 0.5\text{ GeV}$. Similarly, for the case of antineutrino, at $E_\nu = 0.2\text{ GeV}$, $\Delta_{F_3^V}$ is $\sim 4\%$ for the free nucleon case as well as in ^{40}Ar evaluated using LFG, which becomes $\sim 1\%$ at $E_\nu = 0.5\text{ GeV}$.

In general there is a large uncertainty associated with the determination of $F_3^V(Q^2)$ and $F_3^A(Q^2)$ form factors. We have also studied uncertainty due to form factor $F_3^V(Q^2)$. Some of the alternative parameterizations of the form factor $F_3^V(Q^2)$ are given in Eqs.18, 19, which have been used for numerical calculations. The results are shown in Fig.13. We find that for neutrino induced process on free nucleon target, the difference in the results for $\Delta_{F_3^V}$ obtained by using two different forms of $F_3^V(Q^2)$ (Form I using Eq. 18, Form II using Eq. 19) is very small. For example, this difference is $\sim 1\%$ at low energies($\sim 0.2\text{ GeV}$) which almost vanishes with the increase in energy. In the case of antineutrino induced reaction on free nucleon, this difference is around 3% at low energies which gradually vanishes with the increase in energy.

2. Second class axial current

The second class axial vector current contributes in the leading order in addition to the contribution proportional to the lepton mass. Therefore, their relative contribution to the $\nu_e(\bar{\nu}_e)$ nucleon scattering could be comparable to the $\nu_\mu(\bar{\nu}_\mu)$ scattering and we study the contribution of second class axial vector form factor to the cross sections. For this we define

$$\delta_{F_3^A}(E_\nu) = \frac{\sigma_{\nu\mu}(F_3^A \neq 0) - \sigma_{\nu\mu}(F_3^A = 0)}{\sigma_{\nu\mu}(F_3^A = 0)}, \quad (44)$$

and similar expression for antineutrino is used. We show the numerical results in Fig.14. These results are presented for the free nucleon case as well as for bound nucleons in ^{40}Ar , and the cross sections are obtained using the expression of the hadronic current with second class axial vector current. This is to point out that the contribution from the

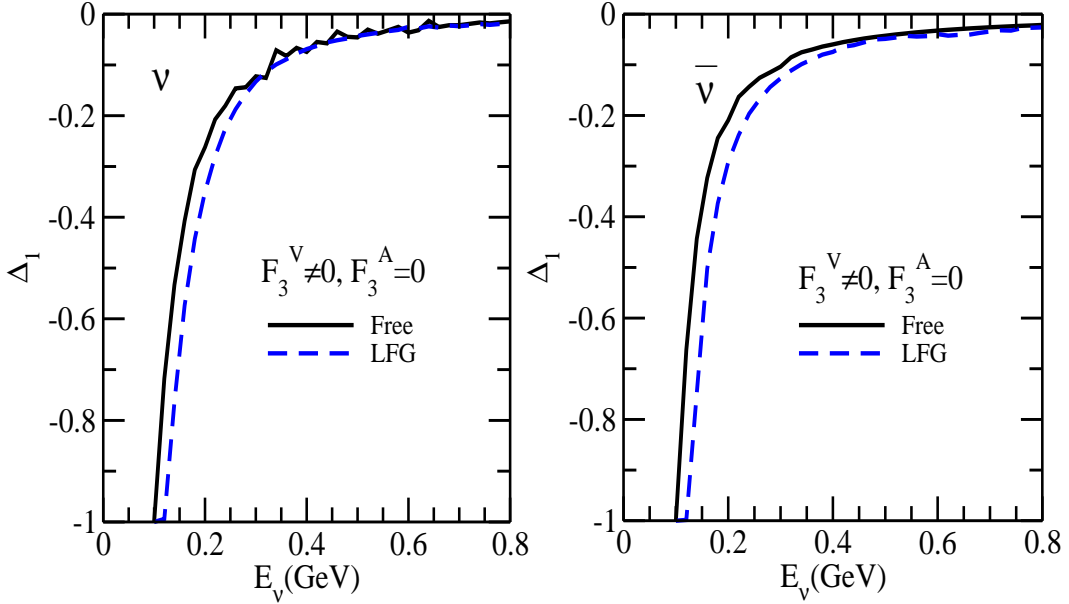


FIG. 11: The difference of fractional changes Δ_1 defined in Eqs.41, for the free nucleon case(solid line), and in ^{40}Ar for neutrino(Left panel) and antineutrino(Right panel) induced processes using LFG(dashed line).

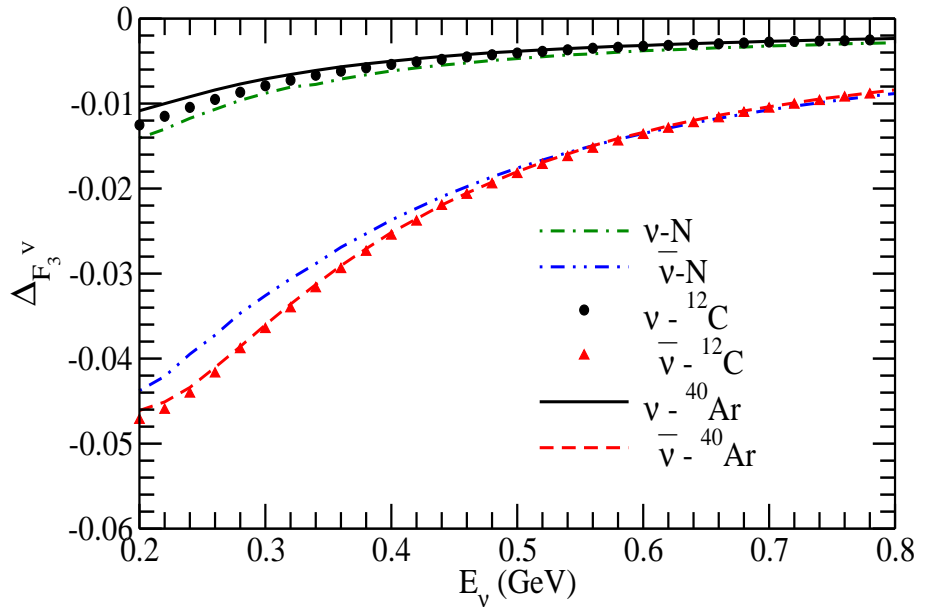


FIG. 12: The difference of fractional changes $\Delta_{F_3^Y}$ defined in Eq.43, for the free nucleon case(neutrino results shown by dashed-dotted line and antineutrino results by dashed-double dotted line) as well as for ^{12}C (circle for neutrino and triangle up for antineutrino) and ^{40}Ar (solid line for neutrino and dashed line for antineutrino) nuclear targets obtained by using LFG.

second class vector current is switched off. We find that $\delta_{F_3^A}$ is hardly sensitive to the presence of $F_3^A(Q^2)$ in ν_μ and $\bar{\nu}_\mu$ scattering cross sections from free nucleon and nuclear targets. We also study the sensitivity of the electron and

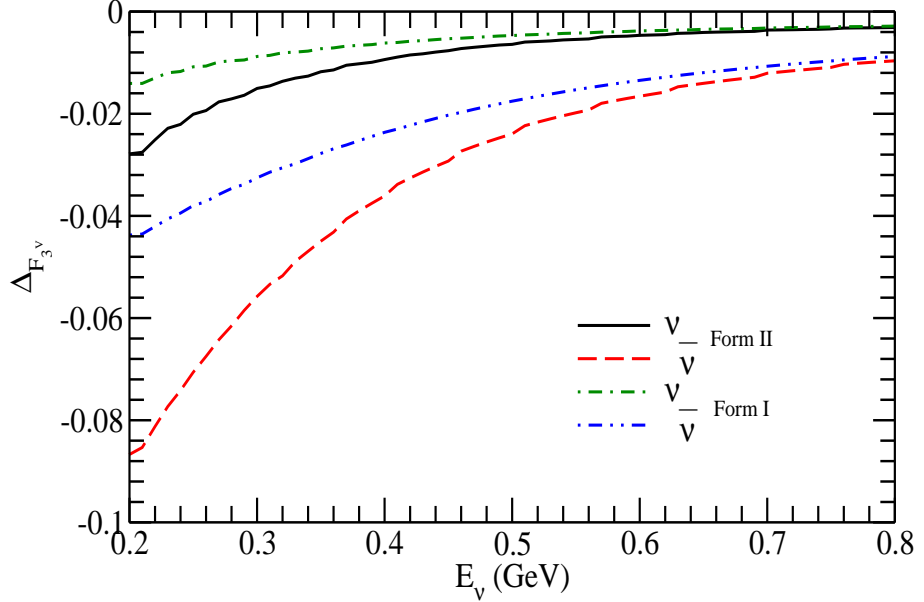


FIG. 13: Variation of $\Delta_{F_3^V}$ as given in Eqs. 43 as a function of (anti)neutrino energies are shown for different forms of $F_3^V(Q^2)$ used in second class currents. We have performed the calculation for (anti)neutrino induced scattering processes on free nucleon target. The results are obtained for Form I and Form II using Eqs. 18 and 19, respectively for $M_A = 1.026 \text{ GeV}$. The results obtained by using Form I for neutrino(antineutrino) are shown by dashed-dotted(dashed-double dotted)line and with Form II are shown by solid(dashed)line, respectively.

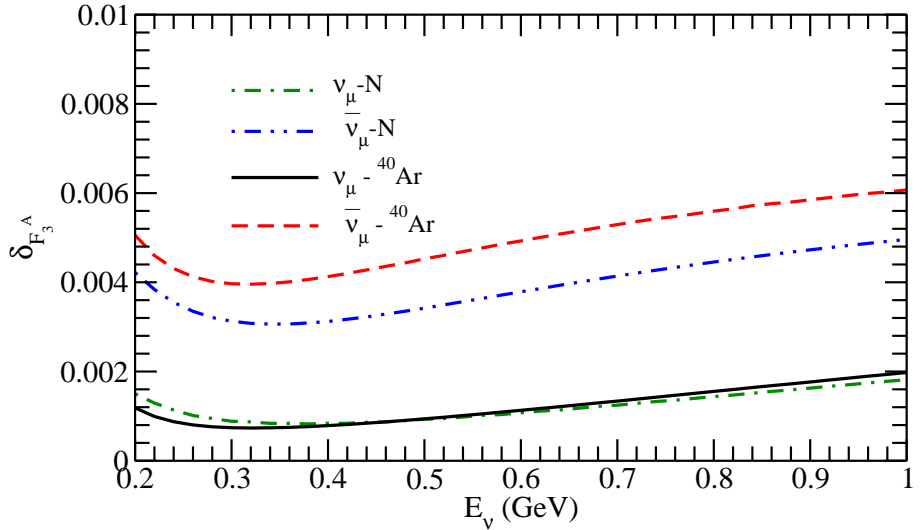


FIG. 14: Results of the fractional change $\delta_{F_3^A}$ defined in Eq.44 as a function of (anti)neutrino energy. The results are shown for the ν_μ induced interaction cross section for the free nucleon case(dashed dotted line), as well as for the nucleons bound in ^{40}Ar (solid line) obtained by using LFG. The results corresponding to $\bar{\nu}_\mu$ induced CCQE process are shown by dashed double dotted line(free nucleon case) and dashed line(^{40}Ar target).

muon production cross sections to $F_3^A(Q^2)$ for free nucleon and nuclei, by defining

$$\Delta_1(E_\nu) = \frac{\sigma_{\nu\mu}(F_3^A \neq 0) - \sigma_{\nu e}(F_3^A \neq 0)}{\sigma_{\nu e}(F_3^A \neq 0)} \quad (45)$$

$$\Delta_2(E_\nu) = \frac{\sigma_{\nu\mu}(F_3^A = 0) - \sigma_{\nu e}(F_3^A = 0)}{\sigma_{\nu e}(F_3^A = 0)} \quad (46)$$

$$\Delta_{F_3^A} = \Delta_1(E_\nu) - \Delta_2(E_\nu), \quad (47)$$

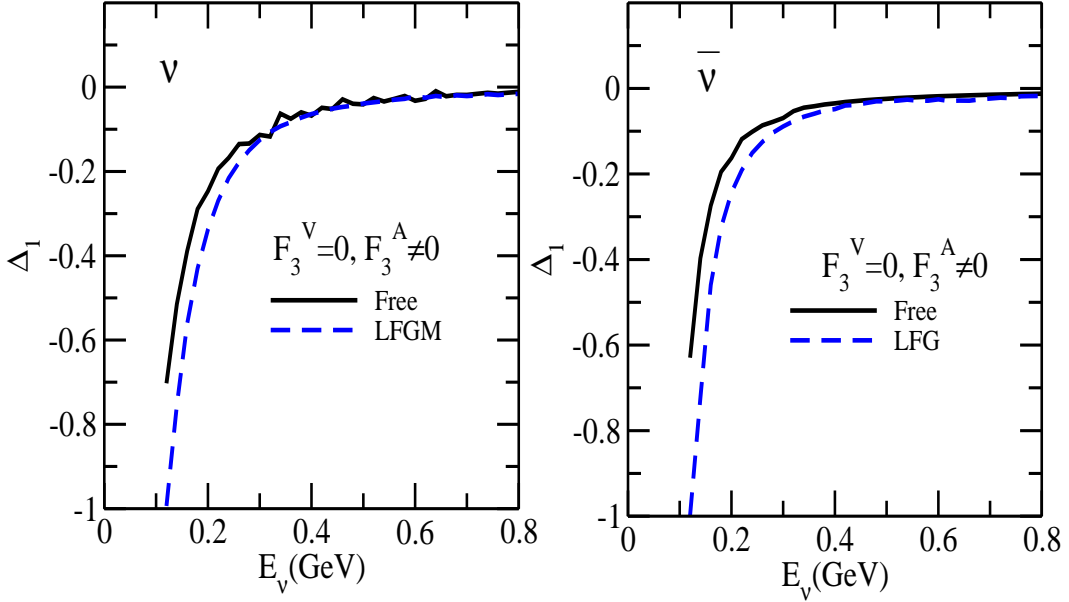


FIG. 15: The difference of fractional changes Δ_1 defined in Eqs.45, for the free nucleon case(solid line), and in ^{40}Ar for neutrino(Left panel) and antineutrino(Right panel) induced processes using LFG(dashed line).

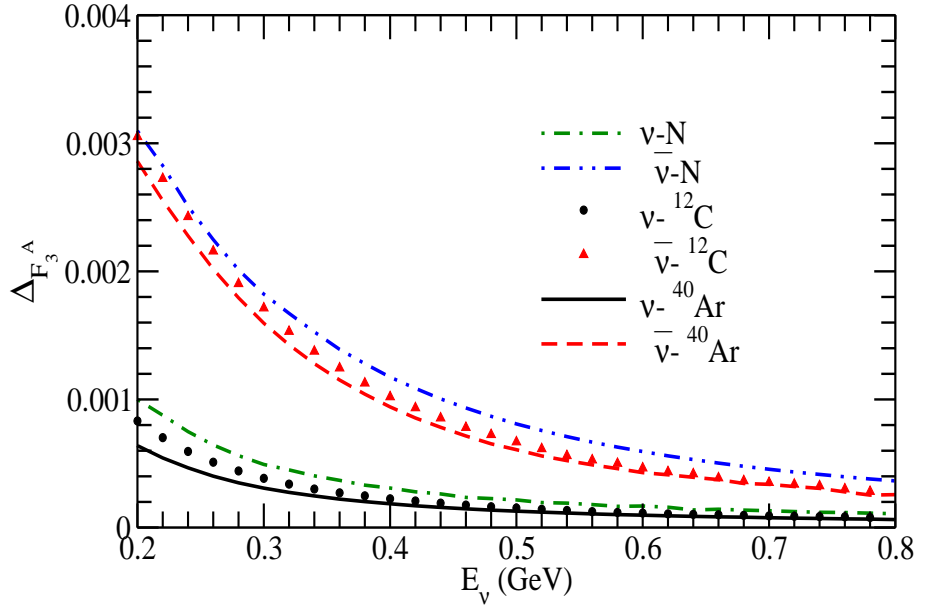


FIG. 16: The difference of fractional changes $\Delta_{F_3^A}$ defined in Eq.47, for the free nucleon case(neutrino results shown by dashed-dotted line and antineutrino results by dashed-double dotted line) as well as for ^{12}C (circle for neutrino and triangle up for antineutrino) and ^{40}Ar (solid line for neutrino and dashed line for antineutrino) obtained by using LFG.

and the numerical results are shown in Fig.15, for $\Delta_1(E_\nu)$. We find the results to be similar in nature as found in the case of currents with second class vector form factor. In Fig. 16, we present the results for $\Delta_{F_3^A}$. In this case also we find the sensitivity to be smaller than observed in the case of $\Delta_{F_3^V}$.

When we compare our present results for the difference in the electron and muon production cross sections on free nucleon target with the results of Day and McFarland [19], we find that our results for the contribution of the $F_3^V(Q^2)$ in the case of antineutrino reactions and the results for the contribution of $F_3^A(Q^2)$ for neutrino reactions agree qualitatively with their results. This is not so in the case of $F_3^V(Q^2)$ for neutrino reactions and $F_3^A(Q^2)$ for

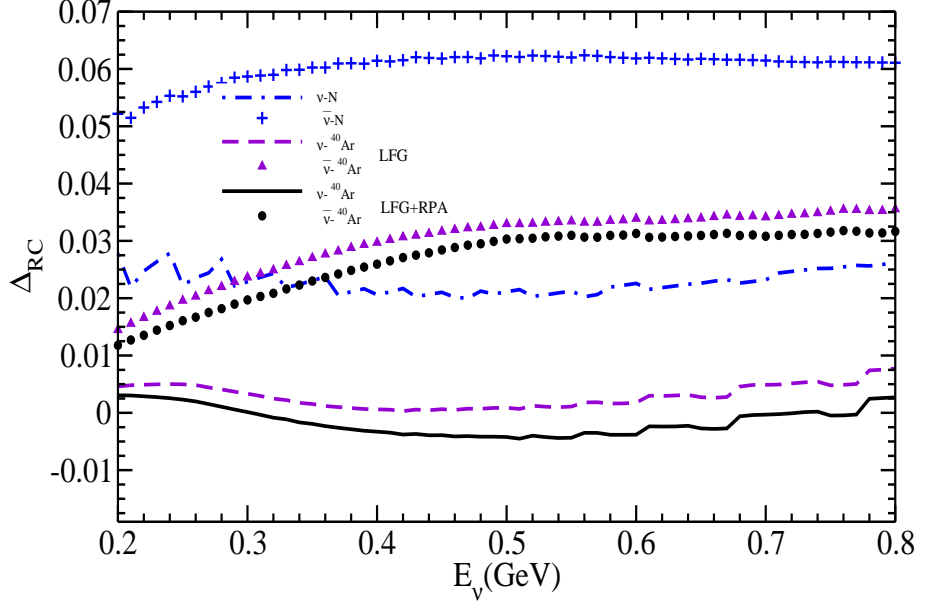


FIG. 17: The effect of radiative corrections on fractional difference Δ_{RC} defined in Eq. 51 for (anti)neutrino induced processes on free nucleon as well as on ^{40}Ar target using LFG with and without RPA effect. For the neutrino(antineutrino) induced processes on free nucleon the results are shown by dashed dotted line(plus), results for calculations using LFG for neutrino(antineutrino) are shown by dashed line (triangle up) and results for calculations using LFG with RPA effect for neutrino(antineutrino) are shown by solid line(circle).

antineutrino reactions.²

E. Radiative corrections

To see the effect of radiative corrections, we have followed the prescription of Rujula et al. [78]. Using this approach [78], one writes the modified cross section as

$$\frac{d\sigma}{dE_l d\Omega_l} \approx \frac{d\sigma_{free}}{dE_l d\Omega_l} + \frac{\alpha}{2\pi} \log \frac{4E_l^{*2}}{m_l^2} \int_0^1 dz \frac{1+z^2}{1-z} \left(\frac{1}{z} \frac{d\sigma_{free}}{dE_l d\Omega_l} \Big|_{\hat{E}_l = \frac{E_l}{z}} \theta(z - z_{min}) - \frac{d\sigma_{free}}{dE_l d\Omega_l} \right), \quad (48)$$

where σ_{free} is the (anti)neutrino induced cross section obtained without radiative effects, E_l^* is the lepton energy in the center of mass frame and z_{min} is given by

$$z_{min} = \frac{4E_l^{*2}}{2ME_\nu} \quad (49)$$

$$\text{with } E_l^* = \frac{s + m_l^2 - M^2}{2\sqrt{s}} \quad (50)$$

where $s = (p + k)^2$ is square of total center of mass energy.

To show the explicit dependence of radiative corrections, we have obtained total scattering cross sections for ν_e and

² This may be due the different expressions used for the contribution of the interference terms between first and second class currents. Our expressions agree with the general expressions given by Pais [76], Kuzmin et al. [77] but not with Eq.(3.18) of Llewellyn Smith [42] which has been used in Ref. [19].

ν_μ induced reactions on free and bound nucleon, with and without radiative corrections and define

$$\begin{aligned}\Delta_1(E_\nu) &= \frac{\sigma_{\nu\mu}(RC) - \sigma_{\nu e}(RC)}{\sigma_{\nu e}(RC)} \\ \Delta_2(E_\nu) &= \frac{\sigma_{\nu\mu}(NR) - \sigma_{\nu e}(NR)}{\sigma_{\nu e}(NR)} \\ \Delta_{RC} &= \Delta_1(E_\nu) - \Delta_2(E_\nu)\end{aligned}\quad (51)$$

where $\sigma_{\nu l}(RC)$, ($l = e, \mu$) represents the cross sections obtained by taking radiative corrections into account and $\sigma_{\nu l}(NR)$, ($l = e, \mu$) are the cross sections without radiative corrections. A similar definition has been used for antineutrino induced process. The results are presented in Fig. 17. These results are shown for the free nucleon target as well as per interacting nucleon in ^{40}Ar , the total cross section for which is obtained by using LFG with and without RPA effect. It may be observed that the effect of radiative corrections on Δ_{RC} depend upon the fact that whether the calculations are performed on free nucleon target or for nucleons bound inside the nucleus. Furthermore, a small dependence on the nuclear models has also been observed. For example, for the neutrino induced process on free nucleon the effect is around 2 % at $E_\nu = 0.5 \text{ GeV}$ while for antineutrino the effect is around 5 % at $E_\nu = 0.5 \text{ GeV}$. When we performed the calculations using Local Fermi Gas Model with and without RPA effect, the effect is same as in the case of free nucleon targets for neutrino scattering. For antineutrino induced process, using Local Fermi Gas Model without RPA effect, it is around 3 %, which becomes $\sim 2\%$ when RPA effect are included.

IV. SUMMARY AND CONCLUSIONS

In the present study we observe the following:

1. $\nu_\mu(\bar{\nu}_\mu)$ induced cross sections in free nucleon as well as nucleons bound in nuclear targets are more suppressed due to threshold effects at low energies than $\nu_e(\bar{\nu}_e)$ induced reaction cross sections. Moreover, when cross sections are evaluated in nuclear targets there is a further reduction in the cross sections due to nuclear medium effects. This reduction is energy dependent. For example, when calculations are performed for ^{12}C nucleus in Local Fermi Gas Model, the cross section for $\nu_e(\bar{\nu}_e)$ induced scattering is reduced by $\sim 30\%(45\%)$ at $E_\nu = 0.3 \text{ GeV}$ from free nucleon case while for $\nu_\mu(\bar{\nu}_\mu)$ induced scattering the reduction is $\sim 32\%(46\%)$ at $E_\nu = 0.3 \text{ GeV}$. Inclusion of RPA correlation with LFG, further reduces the cross section from $\nu_e(\bar{\nu}_e)$ induced scattering by $\sim 37\%(25\%)$ at $E_\nu = 0.3 \text{ GeV}$, which for $\nu_\mu(\bar{\nu}_\mu)$ induced scattering is $\sim 40\%(27\%)$ at $E_\nu = 0.3 \text{ GeV}$. This results in a larger difference in electron and muon production cross sections for the case of nuclear targets as compared to the free nucleon target.
2. At low energies of $E_{\nu/\bar{\nu}} < 0.5 \text{ GeV}$ there is appreciable nuclear model dependence on (anti)neutrino-nucleus cross sections for both flavors of neutrino(antineutrino). The suppression due to nuclear medium effects is larger in the Local Fermi Gas Model(LFG) as compared to the Fermi gas model of Llewellyn Smith [42]. The suppression in the Fermi gas models of Smith and Moniz [41] and Gaisser and O'Connell [43] are larger than LFG. When RPA effects are included in LFG, the suppression is largest.
3. The suppression due to nuclear medium effects is larger in the case of antineutrinos as compared to the cross sections obtained for neutrino induced processes.
4. For a given set of parameters which determine the form factors and other coupling constants the percentage difference in electron and muon production cross sections is more for nuclear targets than for the free nucleon target. This difference decreases with neutrino/antineutrino energy. Also this difference increases with the increase in mass number.
5. The percentage difference in electron and muon production cross sections due to uncertainties in axial dipole mass is more in the case of nuclear targets as compared to free nucleon target. The difference increases with the increase in mass number.
6. The fractional difference in the cross sections due to the presence of pseudoscalar form factor is more in the case of $\bar{\nu}_\mu$ induced CCQE process than ν_μ induced process for the free nucleon case as well as in nuclear targets. Qualitatively at low neutrino energies there is a small difference in the results obtained for the free nucleon target and nucleons bound in nucleus. This difference vanishes with the increase in energy. In the case of antineutrino induced reaction the difference is slightly larger than found in the case of neutrino and this difference does not vanish with the increase in energy. The difference is almost independent of the choice of nuclear target.

The contribution of pseudoscalar form factor in $\nu_\mu(\bar{\nu}_\mu)$ nucleon scattering is about 3%(9%) at low energies of $E_\nu = 0.2 \text{ GeV}$ and becomes $\sim 1\%(3\%)$ at $E_\nu = 0.4 \text{ GeV}$ in the case of free nucleon. When nuclear medium effects are taken into account this contribution increases.

7. The inclusion of second class vector current results in an increase in the total scattering cross section if present experimental limits of the second class form factor $F_3^V(Q^2)$ is used for $\nu_e(\bar{\nu}_e)$ as well as $\nu_\mu(\bar{\nu}_\mu)$ induced processes. With the inclusion of $F_3^V(Q^2)$, $\nu_\mu(\bar{\nu}_\mu)$ induced scattering cross section increases about 1%(4%) for free nucleon case and 1%(8%) when we include RPA with LFG at $E_\nu = 0.4 \text{ GeV}$. For the $\nu_e(\bar{\nu}_e)$ induced processes this effect is smaller than in comparison to $\nu_\mu(\bar{\nu}_\mu)$ induced processes. The difference in electron and muon production cross sections increases at low energies for nuclear targets as compared to the free nucleon target. This difference almost vanishes with the increase in neutrino energy. In the case of antineutrino induced CCQE process this difference is slightly more as compared to the neutrino case. However, this difference is almost independent of the choice of nuclear target.

The effect of including second class axial vector form factor $F_3^A(Q^2)$ (consistent with present experimental limits) is qualitatively similar to the effect of including second class vector form factor but quantitatively quite small as compared to the effect of $F_3^V(Q^2)$ summarized above.

8. The effect of radiative corrections being proportional to $\log(\frac{E^*}{m_l})$ affects the $\nu_e(\bar{\nu}_e)$ scattering cross section more than $\nu_\mu(\bar{\nu}_\mu)$ scattering cross sections when a corresponding charged lepton is in the final state. This gives a difference in $\nu_e(\bar{\nu}_e)$ and $\nu_\mu(\bar{\nu}_\mu)$ scattering cross sections which is almost independent with energy in the case of neutrino induced process while it increases slightly with energy in the case of antineutrino induced process both for the free nucleon as well as the bound nucleons.

A. Acknowledgments

MSA is thankful to Prof. Kevin S. McFarland and some other participants of NuInt14 for showing their interest in this work. MSA is also grateful to the Department of Science and Technology (DST), Government of India, for providing financial assistance under Grant No.SR/S2/HEP-18/2012. FZ acknowledges Maulana Azad National I Fellowship.

Appendix A: Hadronic tensor $J^{\mu\nu}$

1. Relativistic expression for the hadronic tensor $J^{\mu\nu}$

We have followed the prescription of Nieves et al. [46] while taking RPA correlations into account. The difference is that we have also included the contribution coming due to the second class currents. The following is the expression for the hadronic tensor $J^{\mu\nu}$:

$$\begin{aligned}
 J^{\mu\nu} = & 4 \left[(F_1^V)^2 (p^\mu q^\nu + q^\mu p^\nu + 2p^\mu p^\nu + q^2 g^{\mu\nu}/2) - (F_2^V)^2 \left\{ \frac{-q^2 g^{\mu\nu}}{2} + \left(1 + \frac{q^2}{4M^2} \right) \frac{q^\mu q^\nu}{2} \right. \right. \\
 & + \left. \frac{q^2}{4M^2} (p^\mu q^\nu + q^\mu p^\nu + 2p^\mu p^\nu) \right\} + (F_A)^2 \left\{ 2M^2 g^{\mu\nu} \left(\frac{q^2}{4M^2} - 1 \right) + q^\mu p^\nu + p^\mu q^\nu + 2p^\mu p^\nu \right\} \\
 & - (F_P)^2 \frac{q^2 q^\mu q^\nu}{2M^2} + 2(F_3^V)^2 \left(1 - \frac{q^2}{4M^2} \right) q^\mu q^\nu - (F_3^A)^2 \frac{q^2}{2M^2} (2p^\mu + q^\mu) (2p^\nu + q^\nu) \\
 & + F_1^V F_2^V (q^2 g^{\mu\nu} - q^\mu q^\nu) - 2i(F_1^V F_A + F_2^V F_A) \epsilon^{\mu\nu\alpha\beta} p_\alpha q_\beta - 2F_A F_P q^\mu q^\nu \\
 & - F_3^A F_P \frac{q^2}{M^2} (p^\mu q^\nu + q^\mu p^\nu + q^\mu q^\nu) - 2F_3^A F_A (p^\mu q^\nu + q^\mu p^\nu + q^\mu q^\nu) \\
 & \left. \left. + 2F_1^V F_3^V (p^\mu q^\nu + q^\mu p^\nu + q^\mu q^\nu) + F_2^V F_3^V \frac{q^2}{2M^2} (p^\mu q^\nu + q^\mu p^\nu + q^\mu q^\nu) \right] \right] \quad (A1)
 \end{aligned}$$

2. Component form of $J^{\mu\nu}$ incorporating RPA in the lowest order

Here the three momentum transfer \mathbf{q} is taken along Z-axis and RPA is applied in the leading terms. The different components of the hadronic tensors $J^{\mu\nu}$ with RPA effects are

$$\begin{aligned}
J_{\text{RPA}}^{00} = & 4 \left[2(F_1^V)^2 \left(\underline{\mathbf{C_N}} E^2(\vec{p}) + \frac{q^2}{4} + q^0 E(\vec{p}) \right) - \frac{q^2}{2} (F_2^V)^2 \left(\frac{(q^0)^2}{q^2} + \frac{\vec{p}^2 + q^0 E(\vec{p}) + (q^0)^2/4}{M^2} \right) \right. \\
& + 2(F_A)^2 \left(q^0 E(\vec{p}) + \frac{q^2}{4} + \vec{p}^2 \right) - \underline{\mathbf{C_L}} (F_P)^2 \frac{q^2 q_0^2}{2M^2} + 2(F_3^V)^2 (q^0)^2 \left(1 - \frac{q^2}{4M^2} \right) \\
& - (F_3^A)^2 \frac{q^2}{2} \left(\frac{q^0 + 2E(\vec{p})}{M} \right)^2 - \underline{\mathbf{C_N}} F_1^V F_2^V \vec{q}^2 + 2F_1^V F_3^V ((q^0)^2 + 2E(\vec{p})q^0) \\
& + F_2^V F_3^V \frac{q^2}{M^2} \left(E(\vec{p})q^0 + \frac{(q^0)^2}{2} \right) - 2F_P F_A (q^0)^2 - 4F_A F_3^A (E(\vec{p})q^0 + (q^0)^2) \\
& \left. - 2F_P F_3^A \frac{q^2}{M^2} (E(\vec{p})q^0 + (q^0)^2) \right] \tag{A2}
\end{aligned}$$

$$\begin{aligned}
J_{\text{RPA}}^{0z} = & 4 \left[(F_1^V)^2 \left(\underline{\mathbf{C_N}} E(\vec{p}) (2p_z + |\vec{q}|) + q^0 p_z \right) - \frac{q^2}{4} (F_2^V)^2 \left(\frac{E(\vec{p})}{M} \frac{2p_z + |\vec{q}|}{M} + 2 \frac{q^0 |\vec{q}|}{q^2} + \frac{q^0 (2p_z + |\vec{q}|)}{2M^2} \right) \right. \\
& + (F_A)^2 \left(\underline{\mathbf{C_L}} E(\vec{p}) (2p_z + |\vec{q}|) + q^0 p_z \right) - \underline{\mathbf{C_L}} (F_P)^2 q^0 |\vec{q}| \frac{q^2}{2M^2} + 2(F_3^V)^2 q^0 |\vec{q}| \left(1 - \frac{q^2}{4M^2} \right) \\
& - (F_3^A)^2 \frac{q^2}{2M^2} (|\vec{q}| + 2p_z) (q^0 + 2E(\vec{p})) - F_1^V F_2^V q^0 |\vec{q}| + 2F_1^V F_3^V (E(\vec{p}) |\vec{q}| + q^0 p_z + q^0 |\vec{q}|) \\
& + F_2^V F_3^V \frac{q^2}{2M^2} (E(\vec{p}) |\vec{q}| + q^0 p_z + q^0 |\vec{q}|) - 2F_P F_A q^0 |\vec{q}| - 2F_A F_3^A (E(\vec{p}) |\vec{q}| + q^0 p_z + q^0 |\vec{q}|) \\
& \left. - F_P F_3^A \frac{q^2}{M^2} (E(\vec{p}) |\vec{q}| + q^0 p_z + q^0 |\vec{q}|) \right] \tag{A3}
\end{aligned}$$

$$\begin{aligned}
J_{\text{RPA}}^{zz} = & 4 \left[2(F_1^V)^2 \left(p_z^2 + |\vec{q}| p_z - \frac{q^2}{4} \right) - \frac{q^2}{2} (F_2^V)^2 \left(\left(\frac{2p_z + |\vec{q}|}{2M} \right)^2 + \frac{(q^0)^2}{q^2} \right) \right. \\
& + 2(F_A)^2 M^2 \left(\underline{\mathbf{C_L}} + \frac{p_z^2 + |\vec{q}| p_z - q^2/4}{M^2} \right) - \underline{\mathbf{C_L}} (F_P)^2 \frac{q^2 \vec{q}^2}{2M^2} + 2(F_3^V)^2 \vec{q}^2 \left(1 - \frac{q^2}{4M^2} \right) \\
& - (F_3^A)^2 \frac{q^2}{2M^2} (2p_z + |\vec{q}|)^2 - (q^0)^2 F_1^V F_2^V + 2F_1^V F_3^V (2p_z |\vec{q}| + \vec{q}^2) + F_2^V F_3^V \frac{q^2}{2M^2} (2p_z |\vec{q}| + \vec{q}^2) \\
& \left. - F_P F_3^A \frac{q^2}{M^2} (2p_z |\vec{q}| + \vec{q}^2) - 2F_A F_P \vec{q}^2 - 2F_A F_3^A (2p_z |\vec{q}| + \vec{q}^2) \right] \tag{A4}
\end{aligned}$$

$$\begin{aligned}
J_{\text{RPA}}^{xx} = & 4 \left[2(F_1^V)^2 \left(p_x^2 - \frac{q^2}{4} \right) - \frac{q^2}{2} (F_2^V)^2 \left(\underline{\mathbf{C_T}} + \frac{p_x^2}{M^2} \right) + 2F_A^2 M^2 \left(\underline{\mathbf{C_T}} + \frac{p_x^2 - q^2/4}{M^2} \right) \right. \\
& \left. - 2(F_3^A)^2 \frac{q^2 p_x^2}{M^2} - \underline{\mathbf{C_T}} q^2 F_1^V F_2^V \right] \tag{A5}
\end{aligned}$$

$$J_{\text{RPA}}^{xy} = -8iF_A M^2 (F_1^V + F_2^V) (\underline{\mathbf{C_T}} |\vec{q}| E(\vec{p}) - q^0 p_z) \tag{A6}$$

$$\mathbf{C_N} = \frac{1}{|1 - c_0 f'(\rho) U_N(q, k_F)|^2}, \quad \mathbf{C_T} = \frac{1}{|1 - U(q, k_F) V_t(q)|^2}, \quad \mathbf{C_L} = \frac{1}{|1 - U(q, k_F) V_l(q)|^2} \tag{A7}$$

where V_l and V_t are the longitudinal and transverse part of the nucleon-nucleon potential calculated with π and ρ exchanges and are given by

$$\begin{aligned}
V_l(q) = & \frac{f^2}{m_\pi^2} \left\{ \left(\frac{\Lambda_\pi^2 - m_\pi^2}{\Lambda_\pi^2 - q^2} \right)^2 \frac{\vec{q}^2}{q^2 - m_\pi^2} + g' \right\}, \quad \frac{f^2}{4\pi} = 0.08, \quad \Lambda_\pi = 1.2 \text{ GeV}, \quad m_\pi = 0.14 \text{ GeV} \\
V_t(q) = & \frac{f^2}{m_\pi^2} \left\{ C_\rho \left(\frac{\Lambda_\rho^2 - m_\rho^2}{\Lambda_\rho^2 - q^2} \right)^2 \frac{\vec{q}^2}{q^2 - m_\rho^2} + g' \right\}, \quad C_\rho = 2, \quad \Lambda_\rho = 2.5 \text{ GeV}, \quad m_\rho = 0.77 \text{ GeV} \tag{A8}
\end{aligned}$$

g' is the Landau-Migdal parameter taken to be 0.7 which has been used quite successfully to explain many electromagnetic and weak processes in nuclei. $U(q, k_F) = U_N(q, k_F) + U_\Delta(q, k_F)$ is the Lindhard function for the particle-hole excitation and $U_\Delta(q, k_F)$ is the Lindhard function for the delta-hole excitation. The details are given in Ref.[46, 72].

[1] Y. Abe *et al.* [Double Chooz Collaboration], Phys. Rev. Lett. **108**, 131801 (2012).
 [2] J. K. Ahn *et al.* [RENO Collaboration], Phys. Rev. Lett. **108**, 191802 (2012).
 [3] F. P. An *et al.* [Daya Bay Collaboration], Phys. Rev. Lett. **108**, 171803 (2012).
 [4] M. Ericson and M. Martini, Phys. Rev. C **91**, 035501 (2015).
 [5] S. F. King and C. Luhn, Rept. Prog. Phys. **76**, 056201 (2013).
 [6] K. Abe *et al.* [T2K Collaboration] Nucl. Instrum. Meth. A **659**, 106 (2011); <http://t2k-experiment.org/>
 [7] A. Habig [NOvA Collaboration] Nucl. Phys. Proc. Suppl. **229-232**, 460 (2012); <http://www-nova.fnal.gov/>
 [8] S. K. Agarwalla *et al.* [LAGUNA-LBNO Collaboration], arXiv:1412.0804 [hep-ph].
 [9] T. Ishida [Hyper-Kamiokande Working Group Collaboration], arXiv:1311.5287 [hep-ex].
 [10] K. Abe *et al.* [Hyper-Kamiokande Proto-Collaboration], [arXiv:1502.05199 [hep-ex]].
 [11] R. Gran, J. Nieves, F. Sanchez and M. J. Vicente Vacas, Phys. Rev. D **88**, 113007 (2013).
 [12] U. Mosel, O. Lalakulich and K. Gallmeister, Phys. Rev. Lett. **112**, 151802 (2014).
 [13] O. Benhar, P. Huber, C. Mariani and D. Meloni, arXiv:1501.06448 [nucl-th]; O. Benhar, A. Lovato and N. Rocco, arXiv:1502.00887 [nucl-th].
 [14] J. Nieves, I. Ruiz Simo and M. J. Vicente Vacas, Phys. Lett. B **707**, 72 (2012).
 [15] M. Martini, M. Ericson and G. Chanfray, Phys. Rev. C **84**, 055502 (2011).
 [16] M. Martini, M. Ericson and G. Chanfray, Phys. Rev. D **87**, 013009 (2013).
 [17] O. Lalakulich, U. Mosel and K. Gallmeister, Phys. Rev. C **86**, 054606 (2012).
 [18] A. M. Ankowski, O. Benhar and M. Sakuda, Phys. Rev. D **91**, 033005 (2015).
 [19] M. Day and K. S. McFarland, Phys. Rev. D **86**, 053003 (2012).
 [20] L. Fields *et al.* [MINERvA Collaboration], Phys. Rev. Lett. **111**, 022501 (2013).
 [21] V. Lyubushkin *et al.* [NOMAD Collaboration], Eur. Phys. J. C **63**, 355 (2009).
 [22] A. A. Aguilar-Arevalo *et al.* [MiniBooNE Collaboration], Phys. Rev. D **81**, 092005 (2010).
 [23] A. A. Aguilar-Arevalo *et al.* [MiniBooNE Collaboration], Phys. Rev. D **82**, 092005 (2010).
 [24] A. A. Aguilar-Arevalo *et al.* [MiniBooNE Collaboration], Phys. Rev. D **88**, 032001 (2013).
 [25] G. A. Fiorentini *et al.* [MINERvA Collaboration], Phys. Rev. Lett. **111**, 022502 (2013).
 [26] K. Abe *et al.* [T2K Collaboration], Phys. Rev. D **87**, 092003 (2013).
 [27] Y. Nakajima *et al.* [SciBooNE Collaboration], Phys. Rev. D **83**, 012005 (2011).
 [28] R. Gran *et al.* [K2K Collaboration], Phys. Rev. D **74**, 052002 (2006).
 [29] X. Espinal and F. Sanchez, AIP Conf. Proc. **967**, 117 (2007).
 [30] V. Bernard, L. Elouadrhiri and U. G. Meissner, J. Phys. G **28**, R1 (2002).
 [31] V. Bernard, N. Kaiser and U. G. Meissner, Phys. Rev. D **50**, 6899 (1994).
 [32] V. Bernard, H. W. Fearing, T. R. Hemmert and U. G. Meissner, Nucl. Phys. A **635**, 121 (1998) [Nucl. Phys. A **642**, 563 (1998)].
 [33] V. Bernard, T. R. Hemmert and U. G. Meissner, Nucl. Phys. A **686**, 290 (2001).
 [34] M. R. Schindler, T. Fuchs, J. Gegelia and S. Scherer, Phys. Rev. C **75**, 025202 (2007).
 [35] A. Tsapalis, eConf C **070910**, 168 (2007).
 [36] C. Andreopoulos, A. Bell, D. Bhattacharya, F. Cavanna, J. Dobson, S. Dytman, H. Gallagher and P. Guzowski *et al.*, Nucl. Instrum. Meth. A **614**, 87 (2010).
 [37] Y. Hayato, Acta Phys. Polon. B **40**, 2477 (2009).
 [38] D. Casper, Nucl. Phys. Proc. Suppl. **112**, 161 (2002).
 [39] T. Golan, J. T. Sobczyk and J. Zmuda, Nucl. Phys. Proc. Suppl. **229-232**, 499 (2012).
 [40] O. Lalakulich, K. Gallmeister and U. Mosel, J. Phys. Conf. Ser. **408**, 012053 (2013).
 [41] R. A. Smith and E. J. Moniz, Nucl. Phys. B **43**, 605 (1972) [Erratum-ibid. B **101**, 547 (1975)].
 [42] C. H. Llewellyn Smith, Phys. Rept. **3**, 261 (1972).
 [43] T. K. Gaisser and J. S. O'Connell, Phys. Rev. D **34**, 822 (1986).
 [44] S. K. Singh and E. Oset, Nucl. Phys. A **542**, 587 (1992).
 [45] S. K. Singh and E. Oset, Phys. Rev. C **48**, 1246 (1993).
 [46] J. Nieves, J. E. Amaro and M. Valverde, Phys. Rev. C **70**, 055503 (2004) [Phys. Rev. C **72**, 019902 (2005)].
 [47] G. D. Megias, T. W. Donnelly, O. Moreno, C. F. Williamson, J. A. Caballero, R. Gonzlez-Jimnez, A. De Pace and M. B. Barbaro *et al.*, Phys. Rev. D **91**, 073004 (2015); O. Moreno, T. W. Donnelly, J. W. Van Orden and W. P. Ford, Phys. Rev. D **90**, 013014 (2014).
 [48] J. E. Amaro, M. B. Barbaro, J. A. Caballero and T. W. Donnelly, Phys. Rev. C **73**, 035503 (2006).
 [49] H. C. Kim, J. Piekarewicz and C. J. Horowitz, Phys. Rev. C **51**, 2739 (1995).
 [50] A. Meucci and C. Giusti, Phys. Rev. D **89**, 117301 (2014).
 [51] O. Benhar, N. Farina, H. Nakamura, M. Sakuda and R. Seki, Phys. Rev. D **72**, 053005 (2005).

- [52] A. M. Ankowski and J. T. Sobczyk, Phys. Rev. C **74**, 054316 (2006).
- [53] A. V. Butkevich, Phys. Rev. C **85**, 065501 (2012).
- [54] M. Martini, M. Ericson, G. Chanfray and J. Marteau, Phys. Rev. C **80**, 065501 (2009)
- [55] J. Nieves, I. Ruiz Simo and M. J. Vicente Vacas, Phys. Rev. C **83**, 045501 (2011).
- [56] I. Ruiz Simo, C. Albertus, J. E. Amaro, M. B. Barbaro, J. A. Caballero and T. W. Donnelly, Phys. Rev. D **90**, 033012 (2014).
- [57] A. Lovato, S. Gandolfi, J. Carlson, S. C. Pieper and R. Schiavilla, Phys. Rev. Lett. **112**, 182502 (2014).
- [58] J. G. Morfin, J. Nieves and J. T. Sobczyk, Adv. High Energy Phys. **2012**, 934597 (2012).
- [59] L. Alvarez-Ruso, Y. Hayato and J. Nieves, New J. Phys. **16**, 075015 (2014).
- [60] U. Mosel, arXiv:1504.08204 [hep-ex].
- [61] M. Sajjad Athar, S. Chauhan and S. K. Singh, Eur. Phys. J. A **43**, 209 (2010).
- [62] M. Sajjad Athar, S. Chauhan and S. K. Singh, J. Phys. G **37**, 015005 (2010).
- [63] M. Sajjad Athar, S. Ahmad and S. K. Singh, Eur. Phys. J. A **24**, 459 (2005).
- [64] M. Sajjad Athar and S. K. Singh, Phys. Rev. C **61**, 028501 (2000).
- [65] R. Bradford, A. Bodek, H. S. Budd and J. Arrington, Nucl. Phys. Proc. Suppl. **159**, 127 (2006).
- [66] L. A. Ahrens, S. H. Aronson, B. G. Gibbard, M. J. Murtagh, D. H. White, J. L. Callas, D. Cutts and M. Diwan *et al.*, Phys. Lett. B **202**, 284 (1988).
- [67] T. Bhattacharya, V. Cirigliano, S. D. Cohen, A. Filipuzzi, M. Gonzalez-Alonso, M. L. Graesser, R. Gupta and H. W. Lin, Phys. Rev. D **85**, 054512 (2012).
- [68] V. Cirigliano, S. Gardner and B. Holstein, Prog. Part. Nucl. Phys. **71**, 93 (2013).
- [69] C. W. De Jager, H. De Vries and C. De Vries, Atomic data and nuclear data tables, **14**, 479 (1974); H. De Vries, C. W. De Jager and C. De Vries, Atomic data and nuclear data tables, **36**, 495 (1987).
- [70] C. Garcia-Recio, J. Nieves and E. Oset, Nucl. Phys. A **547**, 473 (1992).
- [71] J. Engel, Phys. Rev. C **57**, 2004 (1998).
- [72] E. Oset, D. Strottman, H. Toki and J. Navarro, Phys. Rev. C **48**, 2395 (1993); E. Oset, P. Fernandez de Cordoba, L. L. Salcedo and R. Brockmann, Phys. Rept. **188**, 79 (1990).
- [73] S. Galster, H. Klein, J. Moritz, K. H. Schmidt, D. Wegener and J. Bleckwenn, Nucl. Phys. B **32**, 221 (1971).
- [74] R. Gran [K2K Collaboration], Nucl. Phys. Proc. Suppl. **221**, 98 (2011).
- [75] K. Abe *et al.* [T2K Collaboration], arXiv:1411.6264 [hep-ex].
- [76] A. Pais, Annals Phys. **63**, 361 (1971).
- [77] K. S. Kuzmin, V. V. Lyubushkin and V. A. Naumov, Eur. Phys. J. C **54**, 517 (2008).
- [78] A. De Rujula, R. Petronzio and A. Savoy-Navarro, Nucl. Phys. B **154**, 394 (1979).